1993

Time resolved measurements of light produced by onset of plasma formation on electrodes of fast pulsed high voltage diodes

Wright, Charles M.

Monterey, California. Naval Postgraduate School

(2)

NAVAL POSTGRADUATE SCHOOL
Monterey, California

THESIS

TIME RESOLVED MEASUREMENTS OF LIGHT PRODUCED BY ONSET OF PLASMA FORMATION ON ELECTRODES OF FAST PULSED HIGH VOLTAGE DIODES

by

Charles M. Wright

December, 1993

Thesis Advisor: F. Schwirzke

Thesis Co-advisor: X. K. Maruyama

Approved for public release; distribution is unlimited.

REPORT DOCUMENTATION PAGE

Form Approved OMB No. 0704

1. AGENCY USE ONLY *(Leave blank)*	2. REPORT DATE 10 December 1993	3. REPORT TYPE AND DATES COVERED Master's Thesis

4. TITLE AND SUBTITLE TIME RESOLVED MEASUREMENTS OF LIGHT PRODUCED BY ONSET OF PLASMA FORMATION ON ELECTRODES OF FAST PULSED HIGH VOLTAGE DIODES

5. FUNDING NUMBERS

6. AUTHOR(S) Wright, Charles, M.

7. PERFORMING ORGANIZATION NAME(S) AND ADDRESS(ES)
Naval Postgraduate School
Monterey CA 93943-5000

8. PERFORMING ORGANIZATION REPORT NUMBER

9. SPONSORING/MONITORING AGENCY NAME(S) AND ADDRESS(ES)

10. SPONSORING/MONITORING AGENCY REPORT NUMBER

11. SUPPLEMENTARY NOTES The views expressed in this thesis are those of the author and do not reflect the official policy or position of the Department of Defense or the U.S. Government.

12a. DISTRIBUTION/AVAILABILITY STATEMENT
Approved for public release; distribution is unlimited.

12b. DISTRIBUTION CODE
*A

13. ABSTRACT *(maximum 200 words)*
Despite years of research on electrical breakdown of fast pulsed high vacuum diodes, the mechanisms of the process are far from being fully discovered. It is well known that electrical breakdown begins with plasma formation on the electrode surfaces, but there is disagreement on how this occurs. The most widely accepted model, the Explosive Electron Emission model predicts plasma formation on the cathode by means of ohmic heating caused by a field emitted current. Anode plasma formation under this model is explained as due to energy deposition by fast electrons. A new model proposes that adsorbed neutral molecules on the electrode surfaces play a key role in developing the conditions where unipolar arcs cause plasma formation on both electrodes. In this work, simultaneous measurements of the light produced at the electrodes shows that plasma is produced on the anode in less than 2 nanoseconds after it is produced at the cathode. These findings support the new model.

14. SUBJECT TERMS *current density; cathode spot; vacuum diode; space charge; unipolar arc; x-ray			15. NUMBER OF PAGES * 105 16. PRICE CODE
17. SECURITY CLASSIFICATION OF REPORT Unclassified	18. SECURITY CLASSIFICATION OF THIS PAGE Unclassified	19. SECURITY CLASSIFICATION OF ABSTRACT Unclassified	20. LIMITATION OF ABSTRACT UL

NSN 7540-01-280-5500

Standard Form 298 (Rev. 2-89)
Prescribed by ANSI Std. 239-18

Approved for public release; distribution is unlimited.

TIME RESOLVED MEASUREMENTS OF LIGHT PRODUCED BY ONSET OF PLASMA FORMATION ON ELECTRODES OF FAST PULSED HIGH VOLTAGE DIODES

by

Charles M. Wright
Captain, United States Army
B.S., United States Military Academy, 1983

Submitted in partial fulfillment
of the requirements for the degree of

MASTER OF SCIENCE IN PHYSICS

from the

NAVAL POSTGRADUATE SCHOOL
December 1993

Author: [redacted]
Charles M. Wright

Approved by: [redacted]
F. Schwirzke, Thesis Advisor

[redacted]
X. K. Maruyama, Co-advisor

[redacted]
W. B. Colson, Chairman
Department of Physics

ABSTRACT

Despite years of research on electrical breakdown of fast pulsed high vacuum diodes, the mechanisms of the process are far from being fully discovered. It is well known that electrical breakdown begins with plasma formation on the electrode surfaces, but there is disagreement on how this occurs. The most widely accepted model, the Explosive Electron Emission model predicts plasma formation on the cathode by means of ohmic heating caused by a field emitted current. Anode plasma formation under this model is explained as due to energy deposition by fast electrons. A new model proposes that adsorbed neutral molecules on the electrode surfaces play a key role in developing the conditions where unipolar arcs cause plasma formation on both electrodes. In this work, simultaneous measurements of the light produced at the electrodes shows that plasma is produced on the anode in less than 2 nanoseconds after it is produced at the cathode. These findings support the new model.

TABLE OF CONTENTS

ACKNOWLEDGEMENTS

This work was by no means a solo effort. It is the result of much labor by many people. I would like to thank a few of those individuals who helped me the most. Dr. Fred Schwirzke provided the guiding hand for the theoretical portion of this work and taught me a lot about plasma physics. Dr. Xavier Maruyama taught us how to conduct a good experiment, and provided the logistical and administrative support that we needed. Thanks also to Mr. George Jaksha for all the short notice fabrication that was so necessary to the experiment. I would also like to extend my gratitude to Harold Rietdyk and Don Snyder for their help with the Flash X-ray machine. Probably the greatest thanks is due to Mike Callahan, my lab partner, who did more than his fair share when it came to operating all the lab's equipment. To my wife Maria, thank you so much for caring about my work and listening to all my concerns and joys. Thanks for looking after Keith Xavier while I got the work done!

I. INTRODUCTION

Electrical breakdown between charged electrodes has been studied since the 1930's and beginning in the 1960's extensive research has been done on electrical breakdown in fast pulsed high voltage vacuum diodes. From this research, much has been learned about the results of the breakdown process such as field emission of electrons from the cathode, ion emission from the anode, plasma formation and gap closure. However, the mechanisms which cause these events to occur are still not well understood. [Ref.1]

This work focuses on the pre-breakdown processes that occur in the diode, and specifically the plasma formation on the electrode surfaces. Previous work in this field done at the Naval Postgraduate School confirmed the formation of microscopic craters or pits on both the cathode and the anode surfaces after breakdown. This same phenomena occurs on metallic target surfaces by means of laser induced plasma formation. The formation of these craters is explained by Schwirzke's unipolar arcing model [Ref.2]. Hallal [Ref.3] incorporated the unipolar arcing model into a model which describes how the conditions for unipolar arcing occur on a fast pulsed diode. His experimental work compared diode voltage and current parameters to the light signal produced by the combined anode/cathode plasma formations. Willis [Ref.4] was the first to attempt to measure anode and cathode light

signals as separate light sources but due to equipment limitations he could only measure one at a time. The purpose of this experiment was to determine whether the plasma is produced first on the anode or the cathode and to determine any distinguishing characteristics between the two plasmodic formations. To do this requires the simultaneous and distinguishable observation of the light produced on the electrode surfaces. This information is needed to further the understanding of the mechanisms that lead to electrical breakdown. Most studies in this area focus on the cathodic processes because they are believed to dominate activities leading to breakdown [Ref.1]. But knowledge of the anodic processes is necessary to understand how diodes are used as ion sources. Our findings are that plasma formation on the anode occurs about 1.5 nanoseconds after the initial plasma production begins on the cathode. There is evidence that the anode plasma forms almost simultaneously with cathode unipolar arcing. This is in agreement with models proposed by Hallal, Schwirzke and Willis.

II BACKGROUND

A. DESCRIPTION OF THE BREAKDOWN PROCESS

The term breakdown refers to the filling of the diode gap with some conducting medium allowing current to flow with little or no resistance. In a vacuum diode this process begins with the onset of an applied voltage. For a diode with a gap width, d , a voltage differential, Φ , creates a macroscopic electric field, E , given by the relationship

$$E=\frac{\Phi}{d} \qquad 2.1$$

provided that no current is flowing between the electrodes. Previous work has shown that if the electric field becomes strong enough (approximately 10^7 V/m), the resulting Lorentz force can cause a quantum mechanical tunnelling of electrons through the potential barrier binding them to the cathode surface [Ref.1]. The electrons are then accelerated toward the anode. This action is termed *field emission* and normally occurs at microprotrusions on the cathode surface commonly

referred to as *whiskers*. Field emission takes place at the whiskers because their geometry results in an electric field enhancement at the whisker tip from 10 to 100 times the nominal electric field given by Equation 2.1. This enhancement is visually demonstrated in Figure 2.1.

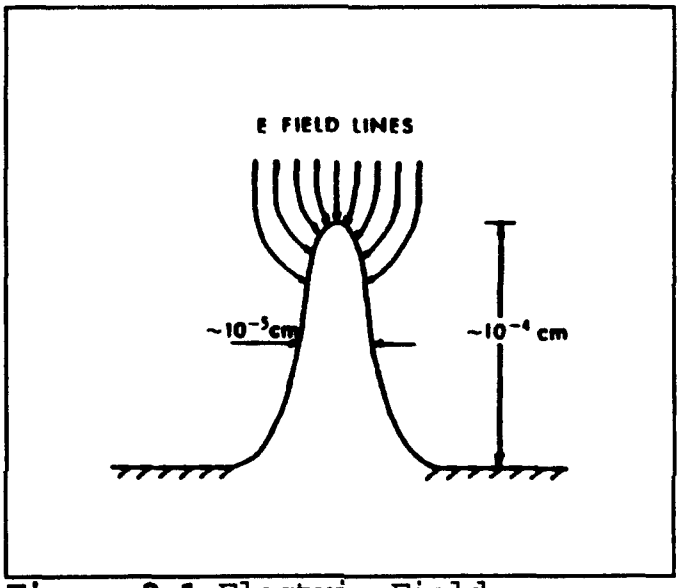

Figure 2.1 Electric Field Enhancement at a Whisker Tip

The current density resulting from field emission is a function of the electric field enhancement factor, β , and the nominal electric field E. Its magnitude is given by the Fowler-Nordheim equation.

$$J_{fe}=C_1\beta^2E^2\exp\left(-\frac{C_2}{\beta E}\right) \qquad 2.2$$

where C_1 and C_2 are constants based on the work function of the material composing the cathode. The next stage of the breakdown process is the explosive formation of plasma on the electrode surfaces. This occurs within a few nanoseconds from the voltage pulse onset. If the explosive like plasma occurs above whiskers on the cathode surface, it is called a *cathode flare*. If it originates near the anode it is an *anode flare* [Ref.5]. The method by which these flares occur is not completely understood and there are several competing theories which attempt to explain these phenomena. Electrode flares are the focus of this work and will be described in detail in later sections.

Electrical breakdown is complete when the plasma produced by electrode flares fills the gap providing a conductive path on which current can flow freely. This happens in a time span much greater than that of plasma production on the electrode surfaces, normally on the order of a few microseconds.

The whole breakdown process was photographed by Hallal [Ref.3] at the Naval Postgraduate School Flash X-ray facility using a video camera with high density filters. Though the photographs do not provide any temporal information, they do provide a good qualitative description of the process. These photographs are shown in Figures 2.2 and 2.3. Figure 2.2 shows two flares originating on the cathode surface. Figure 2.3 shows gap closure (the meeting of a cathode and an anode flare). Based on measurements performed in [Ref.3], gap

closure occurs a few microseconds after plasma production onset.

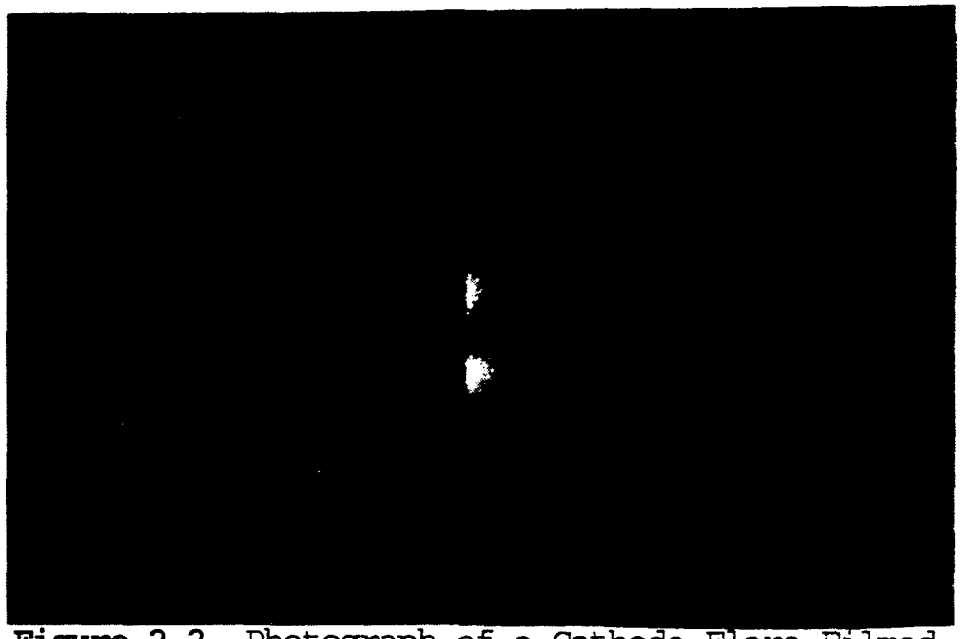

Figure 2.2 Photograph of a Cathode Flare Filmed with a 2% Transmittance Filter. Courtesy Hallal.

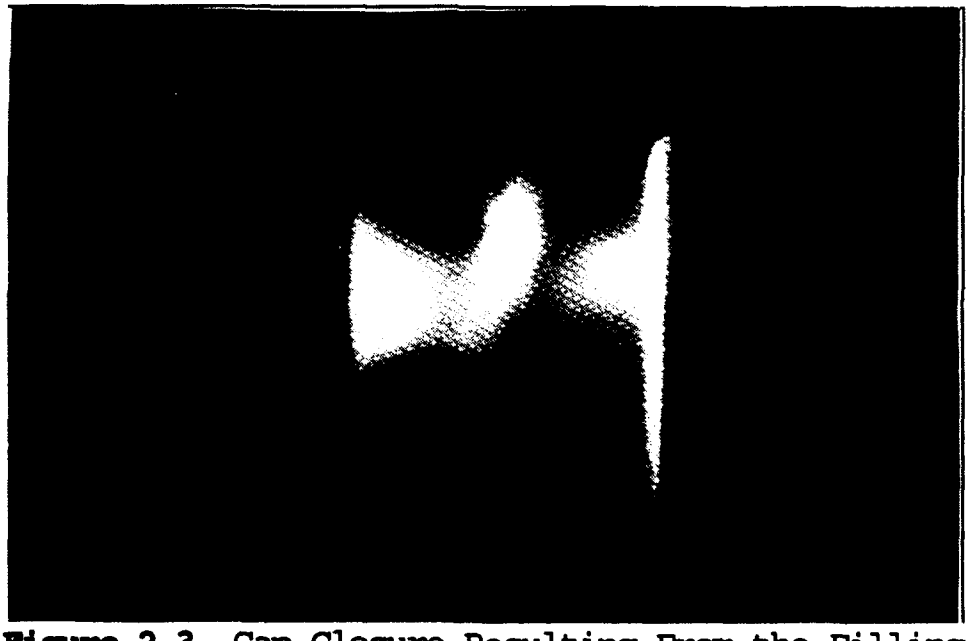

Figure 2.3 Gap Closure Resulting From the Filling of the Diode Gap by Plasma Produced by an Anode and a Cathode Flare.

The material that comprises the plasma cloud obviously originates from the two electrodes and indeed partial dissolution of the electrode surfaces is consistently observed. This dissolution is normally seen in the form of small shallow craters on the electrode surface sometimes referred to as *cathode spots or pitting*. They are normally 10-50 μm in diameter and 1-5 μm deep. A microphotograph (Figure 2.4) taken by Schwirzke of a cathode surface after electrical breakdown shows these spots. Photographs of anode surfaces after electrical breakdown show craters similar in size and shape to those shown in Figure 2.4 [Ref.4].

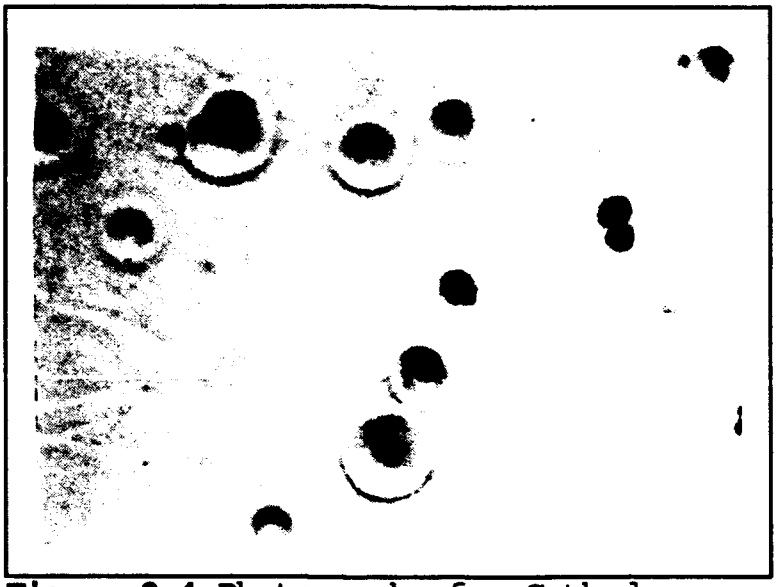

Figure 2.4 Photograph of a Cathode Surface After Breakdown (1000 X).

B. MODELS FOR PLASMA PRODUCTION

1. Explosive Electron Emission Model (Cathode)

A well publicized model for plasma production on the cathode has been proposed by Mesyats [Ref.5]. In this model, the primary mechanism for the formation of cathode flares is simple ohmic heating caused by the field emission current. The model, in brief, explains that after the application of the voltage pulse, field emission of electrons will occur at microprotrusions (whiskers) as discussed in Section A. As the voltage increases, so will the field emission current density until it reaches a critical level where the resultant ohmic heating is sufficient to melt and very quickly vaporize and ionize the whisker. This plasmodic material will then expand in an explosive manner at speeds up to 10^4 m/s.

2. Anode Flares

Mesyats proposes that anode flares occur after cathode flares and are the direct result of energy deposited on the anode surface by the accelerated electrons of the cathode flare. Upper bound calculations based on his experimental conditions (diode gap = 0.35mm, max voltage = 35 kV, and resistance = 150 Ω) show that the energy deposition on the anode surface is sufficient to vaporize the metal in an explosive manner. The Mesyats models also predict a much

brighter anode flare than cathode flare for millimeter gap width diodes. [Ref.5]

C. LIMITATIONS OF THE EXPLOSIVE ELECTRON EMISSION MODEL

The greatest shortcoming of the explosive electron emission (EEE) model is that current densities required to vaporize a whisker in a few nanoseconds is far greater than what is feasible because of space charge limitations. The greater the current density in a vacuum diode gap, the larger the negative charge density is in the gap. The presence of this charge decreases the electric field on the cathode and therefore in a self-regulating manner it reduces the field emission current. The maximum allowable current under space charge limiting conditions is given by the well known nonrelativistic Child-Langmuir law,

$$J_{cl}=\frac{4}{9}\epsilon_o(2\frac{e}{m})^{\frac{1}{2}}\frac{\Phi^{\frac{3}{2}}}{d^2} \qquad 2.3$$

where ϵ_0 is the permittivity constant and e/m is the electron charge to mass ratio.

For a 1 MV potential applied across a 1 inch gap, the Child-Langmuir law limit in a uniform electric field is J_{cl}= 3.6 x 10^6 A/m^2. This current density is far less than the

required current density of 10^{12}-10^{13} A/m^2 to explode the whisker in the 3-10 nanoseconds in which it occurs [Ref.3].

Mesyat's model as it applies to the anode is plausible except that it doesn't explain the formation of anode spots. As mentioned earlier, pitting in the form of anode spots has been observed and the size and depth of these spots is very similar to cathode spots. The question then is how do these similar features occur by different mechanisms as proposed by Mesyats?

III. DESORBED NEUTRAL IONIZATION MODEL

A. OVERVIEW

A new model, termed here the desorbed neutral ionization (DNI) model , has neutral molecules initially adsorbed on the cathode surface playing a key role in the production of cathode flares. Past research [Ref.3] and [Ref.4] have shown it to be successful in predicting the delay time between diode voltage onset and cathode flare occurrence. Also very importantly its principles can also be applied to help understand the mechanism of plasma formation on the anode. The model as it applies to the cathode is presented below much as described in [Ref.3] except that the diode voltage used as an illustration is more representative of the actual diode voltage during plasma production.

B. QUALITATIVE DESCRIPTION (CATHODE)

With the onset of the applied voltage, the resulting current, though initially small, begins to heat the cathode surface. This heating is most intense on the tips of existing whiskers because of the electric field enhancement discussed earlier. The resultant sudden rise in temperature causes the

desorption of an ever present monolayer of neutral contaminant molecules. The composition of these molecules is assumed to be similar to air. At room temperature (300K), air molecules have an average speed of 470 m/s [Ref.6]. They, therefore move away from the cathode at this speed. As the voltage increases, the energy of the field emitted electrons passing through the neutral cloud increases. When the energy of the field emitted electrons is sufficient enough such that the cross section of ionization of the neutrals is appreciable, ionization of the neutrals will occur. The light produced during this ionization is believed to be the initial "spark" of light that signals the onset of plasma production. This sequence of events is depicted schematically in Figures 3.1, 3.2 and 3.3.

The electrons produced by the ionization of neutrals continue to be accelerated to the anode, while the ions moving much more slowly are accelerated back to the cathode where they efficiently transfer energy to the surface causing still more desorption of neutrals. But since the electrons move so much faster than the ions, the ions linger longer in front of the whisker. This results in the formation of a positive space charge sheath a short distance in front of the cathode. The positive sheath increases the electric field on the whisker which increases the amount of field emission electrons. This is often referred to as *enhanced field emission* and is also depicted in Figure 3.3.

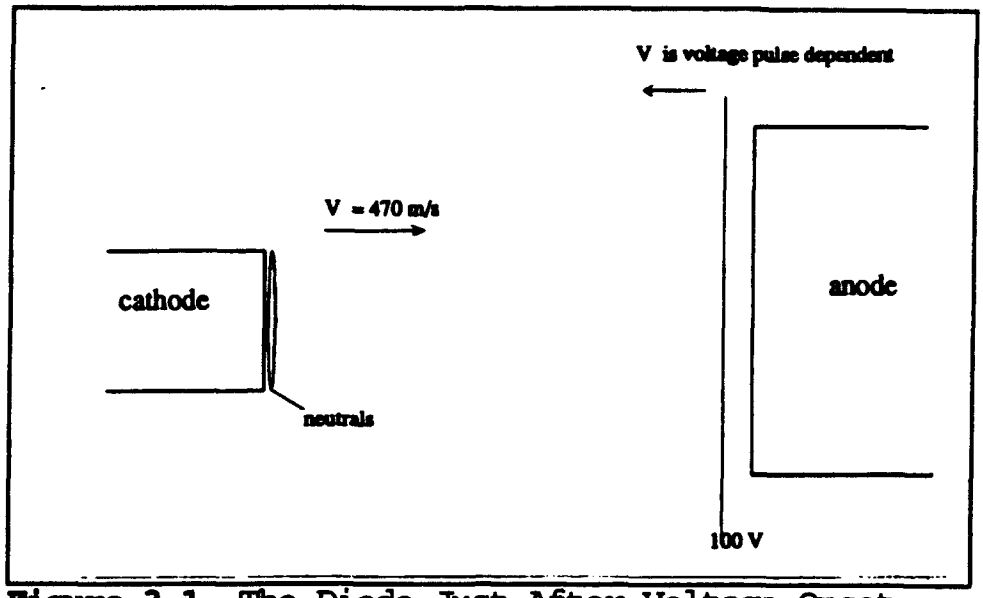

Figure 3.1 The Diode Just After Voltage Onset. Current on the cathode surface causes desorption of neutrals. The diode voltage is not sufficient to cause field emission of electrons.

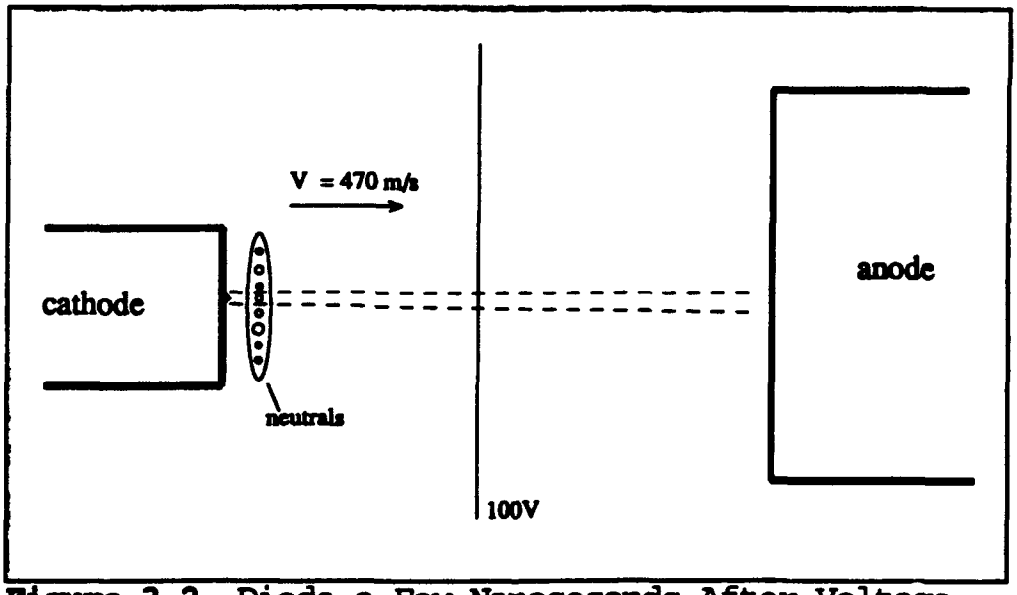

Figure 3.2 Diode a Few Nanoseconds After Voltage Onset. The enhanced electric field on whisker tips is sufficient for field emission of electrons, but electron energy is insufficient to ionize desorbed neutrals.

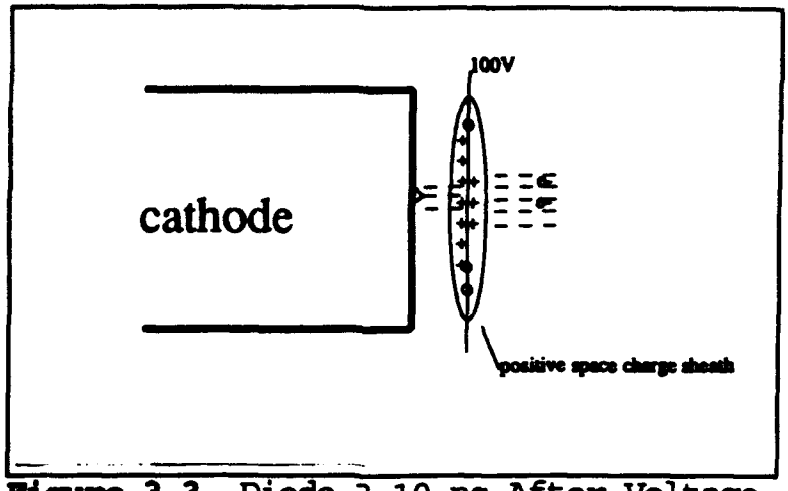

Figure 3.3 Diode 3-10 ns After Voltage Onset. Ionization of the desorbed neutrals has begun by 100 eV electrons and a positive space charge sheath enhances field emission. Unipolar arcing will follow.

The vaporization of the cathode matter and the making of the cathode flare occurs by means of an involved theory [Ref.2]. It will be summarized here for completeness. The field emission current increases, due to ionization of the neutrals, in a self-perpetuating manner until it becomes space charge limited. The continued ionization forms a dense cloud of plasma about the whisker which effectively shields the tip of the whisker from the externally applied electric field. Plasma pressure gradients and sheaths lead naturally to the formation of unipolar arcs that can sustain current densities between the plasma and the cathode surface orders of magnitude larger than the space charge limited, J_{cl} to the anode. This

current combined with massive ion bombardment are believed to be the mechanisms for the formation of explosive cathode flares and the resulting cathode spots or pits.

C. THE MODEL APPLIED (CATHODE)

Using the above described model and applying the conditions and parameters of the diode yields some interesting results and leads much credence to the theory. Experience has shown that the diode voltage at the onset of light is typically around 500 kV and occurs between 4 and 11 nanoseconds after voltage onset. The number of molecules in one adsorbed monolayer is estimated at 2.2×10^{19} particles/m^2. So if at voltage onset, the monolayer becomes desorbed from the cathode surface and they begin moving with a mean velocity of 470 m/s (the average velocity of air molecules at T = 300K [Ref.6]), then at a typical delay time of 10 ns, the majority of the neutrals will have travelled a distance of 4.7 μm. Since the cathode area is 7.9×10^{-4} m^2, the average number of neutrals will be $N = 1.74 \times 10^{16}$ particles in a volume $V = 3.72 \times 10^{-9}$ m^3. This yields an average neutral density $n_o = N/V = 4.7 \times 10^{24}$ particles/m^3, which is about a fifth the density of air at atmospheric pressure. As mentioned earlier, the cross section of ionization of the neutrals becomes appreciable at electron energies of 100 V. When the diode voltage is 500 kV over a 2.54 cm gap, the 100 V equipotential is located 5 μm from the cathode. Therefore the neutrals which have travelled

the 5 μm from the cathode have a high probability of being ionized by field emitted electrons and plasma production at the cathode has begun. Thus Hallal [Ref.3] showed that it was possible to predict the delay time between voltage onset and light production. This was accomplished by determining the intersection of a 100 V equipotential surface (EPS) curve and a neutral cloud position curve. When a significant neutral particle density and electrons with enough energy (100 V) to ionize these neutrals coincide, intense ionization is expected. The 100 V equipotential surface curves shown in Figures 3.4-3.6 are functions of typical diode voltages. If the cathode and anode surfaces are large compared to the separation distance, d , then the electric field between the electrodes is constant and the relation

$$\frac{x}{d} = \frac{V(x,t)}{\Phi(t)} \qquad 3.1$$

describes the location, x , from the cathode of a potential V(x,t) at a time, t , when a potential, $\Phi(t)$, is applied to the anode. Equation 3.1 is used to plot the "EPS" curves shown in Figures 3.4-3.6 and the neutral distance curves, on these same figures are simply a linear plot of position based on an average velocity of 470 m/s. The predicted delay time between diode voltage onset and light onset is the

intersection of these two curves. This intersection point is indicated on each of the graphs.

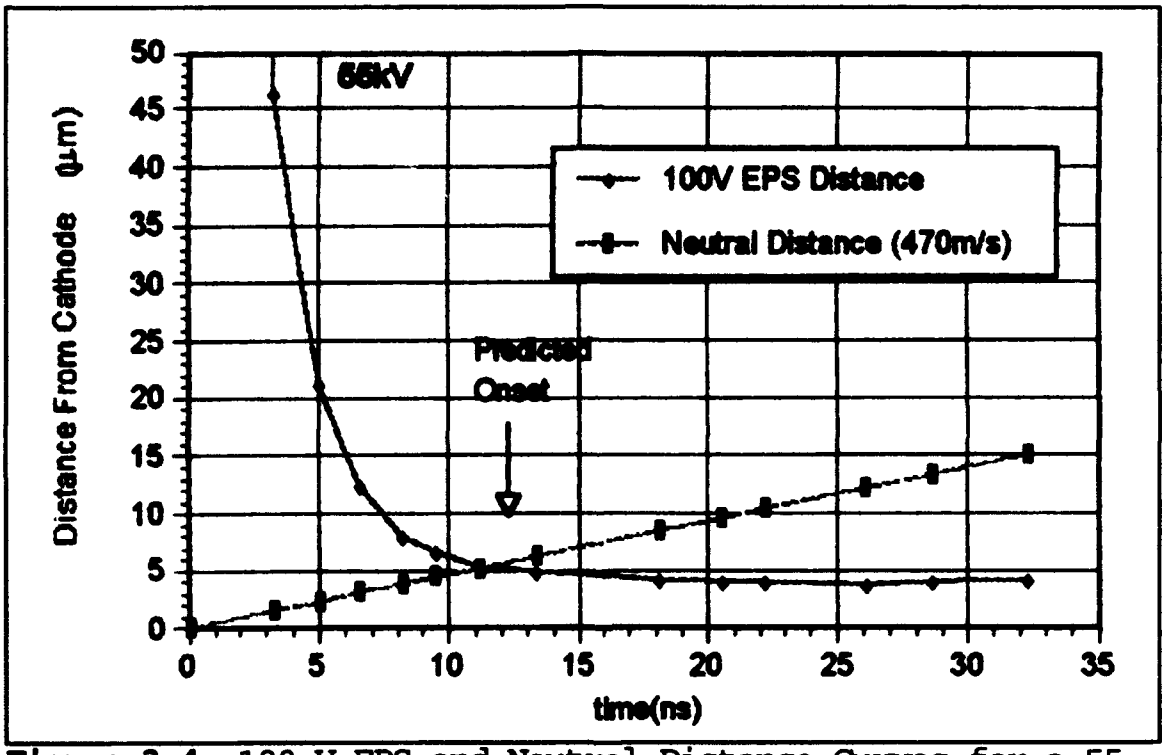

Figure 3.4 100 V EPS and Neutral Distance Curves for a 55 kV Marx shot. The predicted onset time indicated is 11 ns.

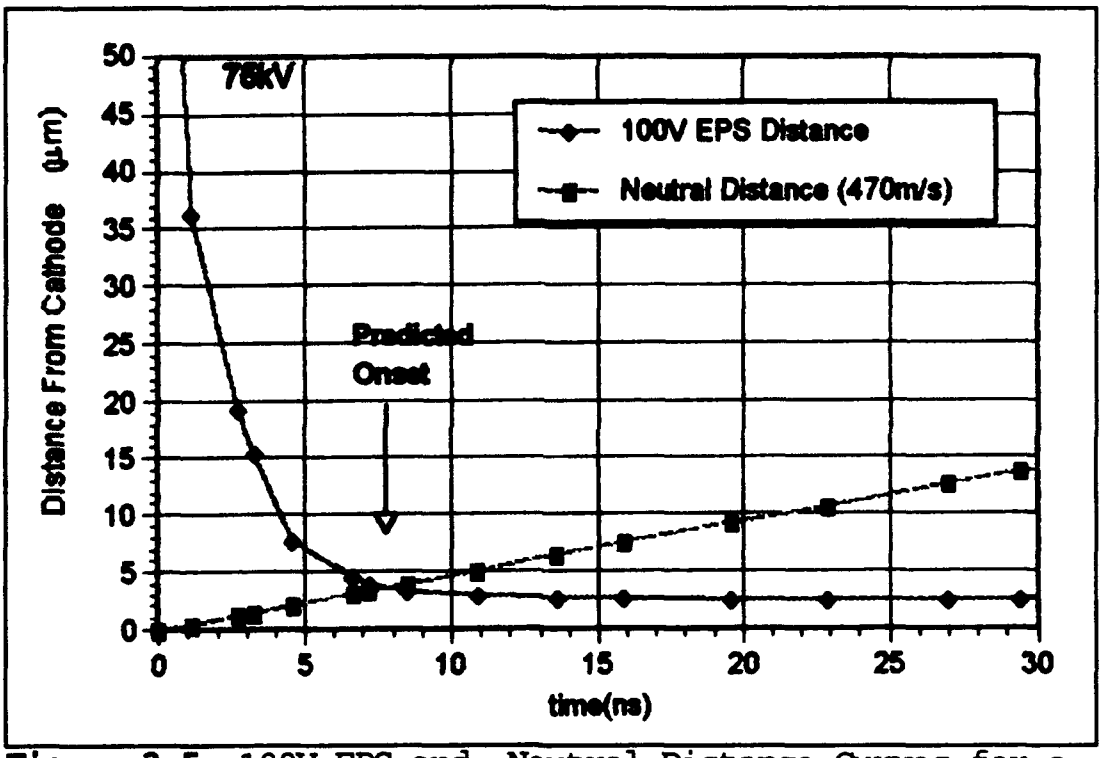

Figure 3.5 100V EPS and Neutral Distance Curves for a 75 kV Marx Shot. The predicted light onset is 7.5 ns.

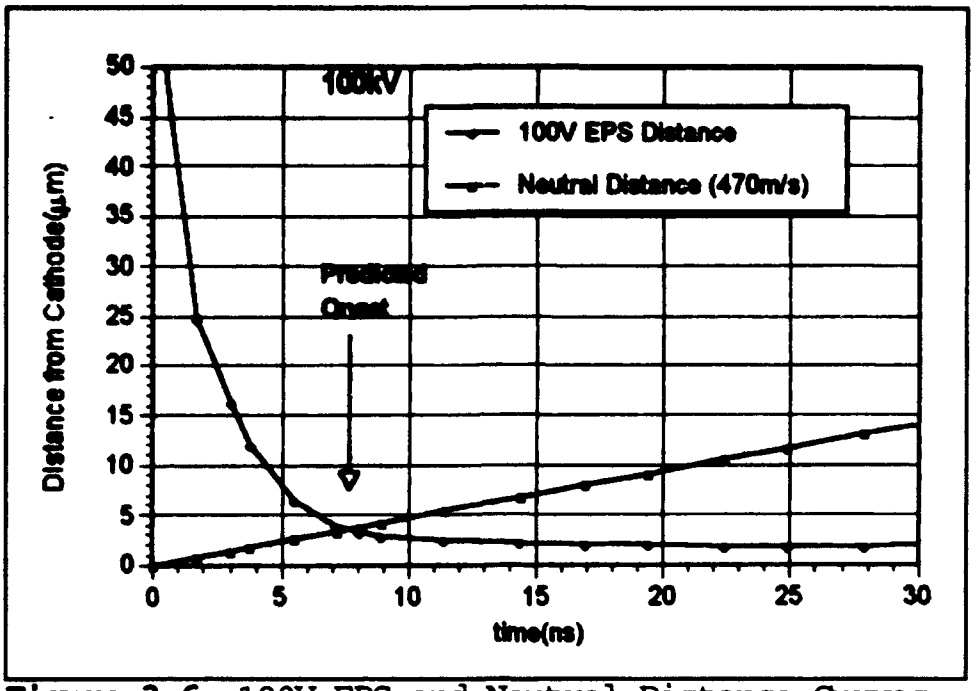

Figure 3.6 100V EPS and Neutral Distance Curves for a 100 kV Marx shot. The predicted light onset time is 7.5 ns.

From the Figures 3.4-3.6 we can predict that the onset of light should occur 11, 7.5 and 7.5 nanoseconds after voltage onset for the 55 kV, 75 kV and 100 kV Marx voltage pulses respectively. These same graphs also predict corresponding neutral particle/100V equipotential location distances of 5 μm, 3.8 μm and 3.6 μm. Based on these locations of the 100 V equipotentials, predicted diode voltages at light onset are: 508 kV (for 55 kV Marx), 668 kV (for 75 kV Marx) and 705 kV (for 100 kV Marx). We should also expect the light created by the neutral ionization to be shortly followed by the much brighter cluster of unipolar arcs (cathode flares).

D. THE MODEL APPLIED TO THE ANODE

Because anode spots (small craters) have been consistently observed [Ref.4], it is believed that the same mechanism that creates spots on the cathode is responsible for anode spots. This requires that a sheath , positive with respect to the anode, forms which results in field emission above a whisker as described above for the cathode. One method by which this could occur was proposed by Willis [Ref.4]. In summary, he suggested that the huge flux of high energy electrons from the cathode flare plasma strikes adsorbed neutrals on the anode surface and this causes some ionization of the neutrals. Though the cross section of ionization for high energy electrons is very small, the electron flux and neutral density on the surface are sufficient to produce a strong enough ionization rate to cause a positive space charge sheath to form a few micrometers from the anode. This positive sheath has enough charge to have a potential above that of the applied anode voltage. This is possible because of the relatively large inertia of the ions. Ion flight time to the cathode is about 10 ns, while the time it takes secondary electrons to travel a few microns to the anode is less than 1/1000 of a nanosecond. At sufficiently high ionization rates, *field reversal* and eventually field emission from the anode and unipolar arcing will occur.

The required net ion density (ions/m^2) above the anode to cause field reversal can be estimated using the parallel capacitor electric field relationship

$$E = \frac{\sigma}{\epsilon_o} \qquad 3.2$$

Where σ is the ion space charge layer density (C/m^2) and ϵ_0 is the permittivity constant. For an applied voltage of 500 kV over a 2.54 cm gap (E = +2 x 10^7 V/m), field cancellation (E = 0) occurs if $\sigma = E\epsilon_o$ = 1.77 x 10^{-4} C/m or an ion sheath consisting of 1.1 x 10^{15} ions/m^2. To create complete field reversal with an electric field strength of E = -2 x 10^7 V/m (which is sufficient for the onset of field emission from the "anode" surface) it takes twice that value or 2.2 x 10^{15} ions/m^2. When this value is achieved, unipolar arcing can occur and a plasma layer forms in front of the anode.

A variation to the model presented by Willis [Ref.4] is that one of the many monolayers is desorbed from the anode surface and like that which occurs on the cathode the neutrals travel away at an average speed of 470 m/s. These neutrals are then ionized by several means including the high energy (500 keV) electron energy flux. This sets off a chain of events which leads to the formation of an ion sheath which has a greater potential than the anode.

It is not believed that the high energy electron flux by itself can cause sufficient ionization of the neutral cloud in front of the anode to create field reversal. This is because of the small cross section of ionization at such high energies. One way to estimate the ionization rate created by the high energy electrons is to assume that the cathode flare produces a flux of electrons that is large enough to become space charge limited. So applying equation 2.3, we can estimate a current density of $J_{cl} = 1.27 \times 10^6$ A/m^2. This is equivalent to an electron flux of $F_e = 7.9 \times 10^{25}$ e$^-$/m^2-s. For many gases the cross section of ionization by high energy electrons is $\approx 10^{-22}$ m^2 [Ref.7]. With the same average density of the neutral cloud as calculated for the cathode of $n_o = 4.7 \times 10^{24}$ particles/m^3, the electrons mean free path is $\lambda = 1/n_o\sigma = 2 \times 10^{-3}$ m. This is a long mean free path and ionizes the 4.7 μm thick cloud with an efficiency of $\eta = 4.7\ \mu m / \lambda = 2.35 \times 10^{-3}$ ionizations/e$^-$. The ionization rate is then $R_{ionization} = \eta F_e = 1.86 \times 10^{22}$ ionizations/m^2-s or on a nanosecond time scale $R_{ionization} = 1.86 \times 10^{13}$ ionizations/m^2-ns. At this rate, even if the ions were stationary(flight time to the anode is $\approx$ 10 ns), it would take at least 120 ns to create an ion sheath of 2.2×10^{15} ions/m^2 (required for a 2×10^7 V/m field reversal). So it is necessary that there be other ionizing sources and mechanisms that must take place to speed up field reversal.

A plausible sequence of events leading to field reversal is described here. There are actually two other ionization

mechanisms. The first is ionizing radiation created in the cathode plasma. Particularly effective is radiation in the ultra violet band. The exact amount of ionizing radiation produced, however, is unknown. The other ionization source is *secondary electrons* produced by any of the ionization processes. These electrons are much slower than the high energy flux electrons so they are a much more efficient ionization source for nearby neutrals in the cloud. More importantly, these electrons are produced at a location that is initially about 100 V lower than the anode, so they strike adsorbed neutrals still on the surface with 100 eV. The cross section of ionization for air molecules by 100 eV electrons is $\approx 10^{-20}$ m^2 [Ref.7] or 100 times that of 500 keV electrons. Based on the assumed adsorbed (still on the anode surface) neutral density of $\sigma_0 = 2.2 \times 10^{19}$ m^{-2}, we know that the spacing between neutrals is $\approx 2 \times 10^{-10}$ m. Therefore the volumetric density of adsorbed neutrals is $n = \sigma_o/2 \times 10^{-10}$ m $= 10^{29}$ m^{-3}. With the cross section of the neutrals to the 100 eV electrons being 10^{-20} m^2, the corresponding mean free path of the secondary electrons in the adsorbed "swamp" is $\lambda = 1/n\sigma \approx 10$ angstroms. This is about the thickness of several monolayers of neutrals. So almost every secondary electron will ionize a surface neutral and on the average they would be expected to penetrate several monolayers before ionization will occur. The imbedded ions are then pulled toward the cathode. They will likely collide with a number of neutrals on their way off the

surface. Momentum transfer here is very efficient because of the like sizes of the ions and the adsorbed neutrals. The added energy will overcome the Van der Waals bonds and there will be a burst of neutrals from the surface. This will greatly increase the neutral density in the cloud above the anode and avalanche ionization can be expected by the ionization means discussed earlier. This process is shown in Figures 3.7 and 3.8.

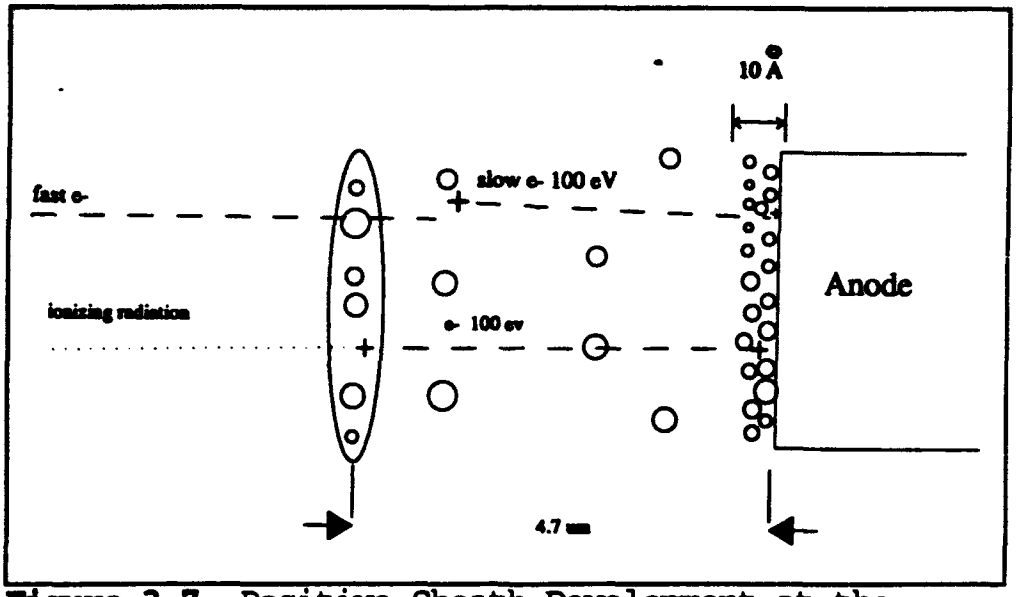

Figure 3.7 Positive Sheath Development at the Anode. Secondary electrons efficiently ionize desorbed neutrals on the anode surface.

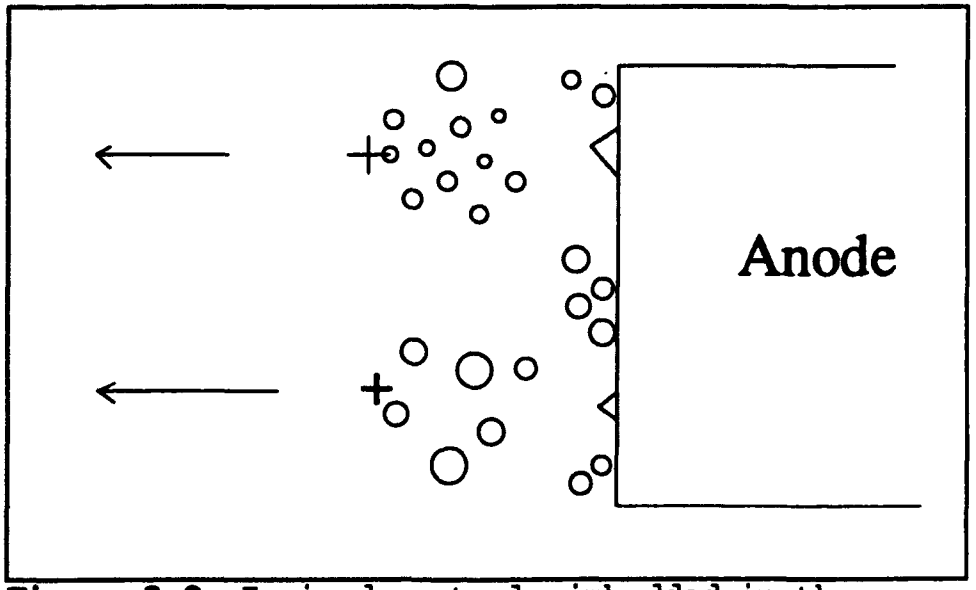

Figure 3.8 Ionized neutrals imbedded in the neutral "Swamp" are pulled toward the cathode and collide with neutrals on their way.

After ionization becomes sufficient for field reversal, the diode should have a voltage profile similar to Figure 3.9. Note the raised potentials near the electrode surfaces. The straight line is what the potential would be in the absence of the plasma sheaths in the gap. The slow ions created by ionization of the neutrals provide the space charge layers (and higher potentials) in front of both the anode and the cathode.

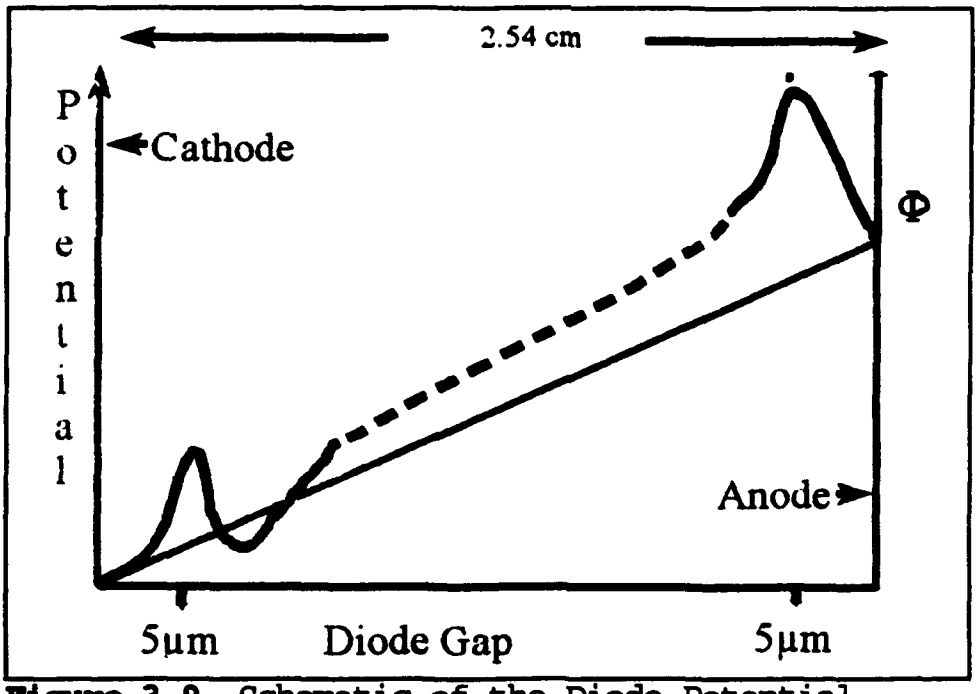

Figure 3.9 Schematic of the Diode Potential

E. A TIME PREDICTION OF ANODE FLARES

By looking at the duration times of the individual processes involved in the formation of anode flares as described above, it is possible to obtain an order of magnitude estimate of the time interval between onset of the cathode flare and onset of the anode flare. The initiating event at the anode is the onslaught of the high energy electrons and ionizing radiation into the already existing neutral cloud. The electrons are highly relativistic travelling at ≥ 0.9 c, so travelling across the 2.54 cm gap, both ionizing sources reach the anode in less than 1/10 of a nanosecond. The slow secondary electrons accelerated by a 100 V potential, from 5 μm away from the anode travel for only 1/1000 of a nanosecond before striking and ionizing neutrals on the anode surface. These ions, imbedded in the "swamp" of neutrals, are initially accelerated in the direction of the cathode by an electric field of $E = 2 \times 10^7$ V/m. This gives an oxygen ion an acceleration of $a = 1.25 \times 10^{14}$ m/s^2, so the time to travel from rest a distance, s, is

$$t=\sqrt{\frac{2s}{a}} \qquad 3.3$$

The ion sheath must be located above the whisker tip in order for it to cause field reversal on the whisker. So both the imbedded ions and the surrounding neutrals must clear a

typical whisker tip distance of s ≈ 1 μm before field reversal can take place. Applying equation 3.3 to the ions gives a time of flight for the ions to a distance above the whisker tip of 0.126 nanoseconds. For any neutrals that have not yet been ionized, their transit time to the sheath area can be estimated by assuming they have at least an average speed of 470 m/s. Travelling with this speed it will take the neutrals about 2 ns to enter the sheath. Because of avalanche ionization conditions, we would expect most of these neutrals to be ionized before that time, but it is a good high end estimate. The neutral travel time above the whisker tip can then be considered the limiting event. We can therefore expect anode plasma formation between 0.1 and 2 nanoseconds of the cathode flare.

IV. EXPERIMENT

A. OVERVIEW

This experiment is designed to determine the time scale of five important plasma formation parameters. The parameters to be measured were: diode voltage, diode current, anode and cathode light pulses, and the breakdown x-ray signal. The setup was used for two different experiments; one studying the temporal response of visible light produced at the anode and cathode, and the second studying the correlation between visible light produced at the cathode and the resulting x-ray pulse that occurs when the electrons emitted from the cathode plasma reach the anode. Both experiments compare the onset of plasma formation to the voltage pulse onset and relate these to the model in Chapter III.

The need to determine all five parameters on the same firing of the flash x-ray (FXR) machine made the setup very complex. To simplify the description, the experimental setup is divided into electrical, optical and x-ray component setups. Two different optical setups were used to record data. Both setups are described below.

B. EXPERIMENTAL SETUP

1. Equipment and Laboratory Layout

This experiment was performed at the Naval Postgraduate School (NPS) Flash X-ray (FXR) facility using a Physics International Company Pulserad 112A Flash X-ray machine. A layout of the FXR facility is shown in Fig 4.1 [Ref.8]. The pulserad 112A generates voltage pulses with pulse durations of 20-25 nanoseconds full width half maximum (FWHM) and peak voltages between 600 kV and 1.6 MV across a high vacuum (10^{-5} - 10^{-6} Torr) diode. The diode gap for the pulserad is 2.54 cm, and the cathode is stainless steel. The anode used was 15 mil tantalum for x-ray creation. Later, a solid stainless steel anode was used to further examine the anode and cathode light pulses and damage mechanisms. For a complete description of the Pulserad 112A see [Ref.9].

The diode voltage was measured by PIM 197A25 voltage divider and the diode current was measured by a PIM199B B-dot sensor, both made by Physics International. The signals from these monitors were measured by Tektronix 7104 1 GHz oscilloscopes and Tektronix Digital Camera Systems (DCS). The voltage signal required 46dB attenuation, and the current 20dB attenuation to be viewed on the oscilloscopes. The absolute magnitudes of these signals have significance in this experiment so they must be calculated based on the oscilloscope trace. Actual diode voltage is determined by V_{ac}=

320 V_{scope} [kV] and diode current is determined by I_{ac}[kA] = 7.31 V_{scope} [Ref.9].

Fast rise time (0.4 ns) photo detectors with optical fiber input were used to measure the plasma light signals, and a foil shielded photodetector (400 ps rise time) was used to measure the x-ray pulse. The anode, cathode, and x-ray signals were measured using two Tektronix DSA 602A digital signal analyzers (DSA) with 1 GHz bandwidth. Table 4.1 shows the detection and measurement equipment used and its important operating characteristics.

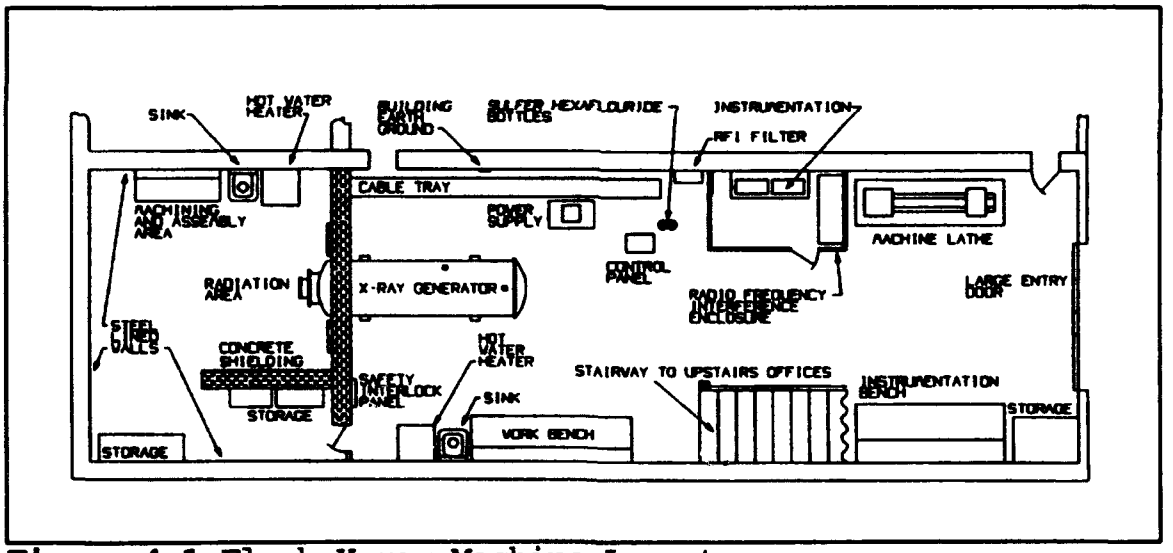

Figure 4.1 Flash X-ray Machine Layout

Table 4.1 DETECTION AND MEASURING EQUIPMENT USED FOR EXPERIMENT

Equipment	Purpose	Manufacturer/ Model	Characteristics	Ref.
Photo Detector	Detect Plasma Light Pulse	NewFocus/ Model 1601	1GHz BW ±15V Bias 400ps Risetime	10
X-ray Detector	Detect X-ray pulse	Lasermetrics/ Series 3117 Type I	PIN Silicon 150ps Risetime 100V Reverse Bias	11
Voltage Divider	Detect/Send Voltage Pulse	Physics International/ PIM-197A25	±5% Accuracy 1.6kV/V Sensitivity	9
Fluxmeter	Current Detector	Physics International/ PIM-199B	±5% Accuracy .872kV/T Sensitivity	9
Oscilloscope (2)	Acquires Voltage and Current Waveforms	Tektronix/ 7104 w/7B92A Time Base	1GHz BW ±3% Timebase Accuracy	12
Digitizing Camera System	Measures and Records Oscilloscope Waveforms	Tektronix/ DCS 01	512 Pixels/Sweep Use w/7104 Scopes	13
Digitizing Signal Analyzer	Acquires, Measures, and Records Light and X-ray Waveforms	Tektronix/ DSA 602A w/ 11A34 Plug In	1GHz BW (2 Channel) Disk Drive Storage Spreadsheet Files ±0.03% Timebase Accuracy	14

2. Signal Processing Configuration

The signal processing arrangement allowed simplified data acquisition of five almost simultaneous waveforms. A Stanford Research Digital Delay Generator, DG-535, was used to synchronize the timing of the wave forms. Figure 4.2 shows a schematic drawing of the signal processing setup.

To synchronize the time scales of the measured waveforms, the oscilloscopes and DSAs had to be externally triggered before arrival of their signals. The Marx Bank voltage was used as the base trigger because it occurs about 100 ns before the measured diode end events. The Marx signal then triggers the delay generator, DG 535, which in turn triggers each oscilloscope or DSA. The delays on the DG-535 are set based on a timing procedure covered in the "timing" section. This arrangement insures that the start time for each oscilloscope/DSA is the same.

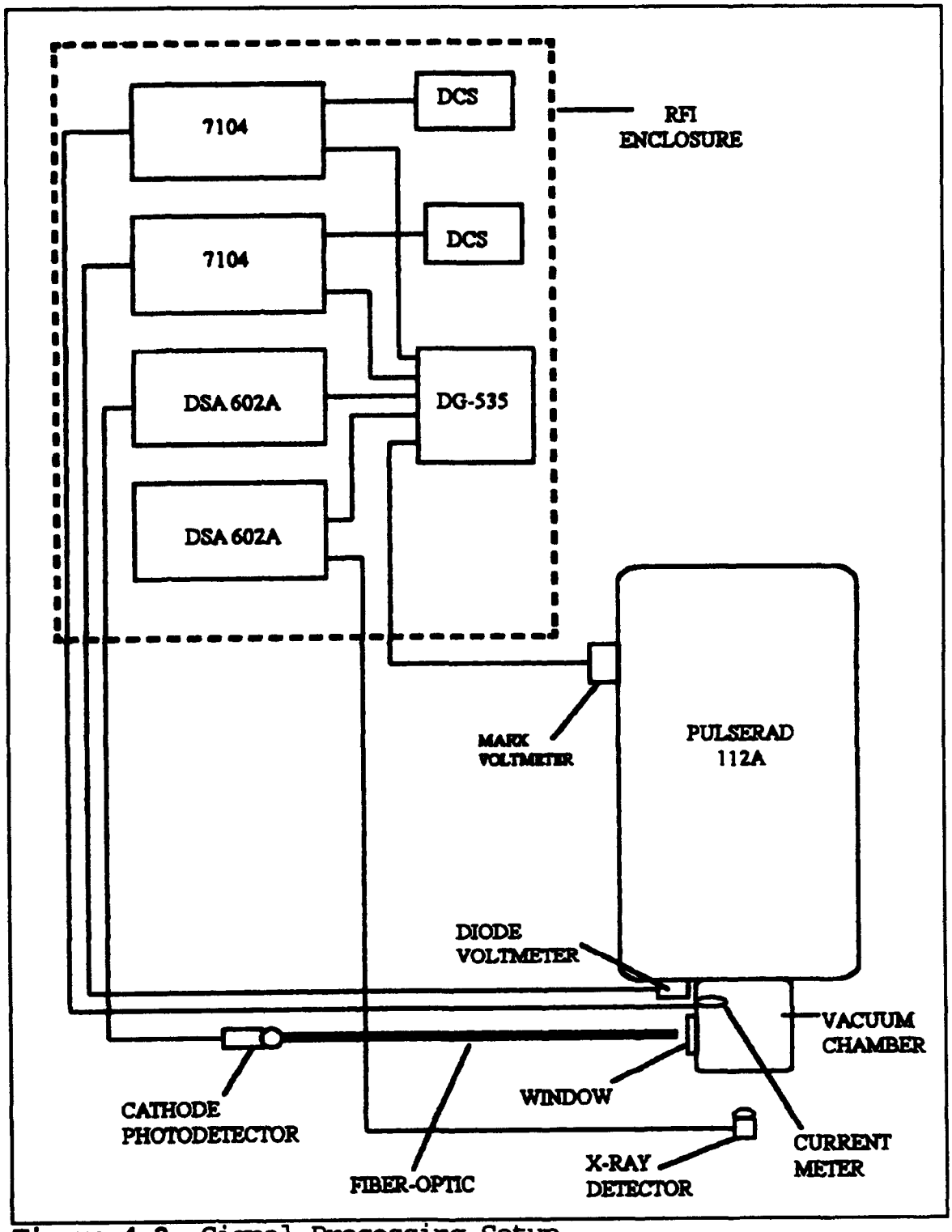

Figure 4.2 Signal Processing Setup

3. Optical Setup 1

The configuration of optical setup 1 is shown in Figure 4.3. The setup used two *New Focus*, Model 1601, photodetectors to convert the light signal produced at the anode and cathode into an electrical signal which could be recorded by the DSA. The detectors were housed in a half inch thick aluminum barrel to reduce electromagnetic noise. They were biased to ± 15 V and their outputs were connected to heavily shielded, high frequency capable, coaxial cables. Each fiber optic bundle, 0.125 inches(0.318 cm) in diameter and six feet (183 cm) long, had one end coupled to the photodetector's optically sensitive area. The other end was fed through drilled holes of a lead brick. The lead bricks were needed to prevent x-rays from registering on the light detectors. This is discussed in greater detail in Section D of this chapter. The protruding ends of the fiber optic cables were then separated by a 1/4 inch thick aluminum plate which was placed flush against the vacuum chamber window and centered on the middle of the diode gap. This plate served to block light produced on the cathode surface from entering the fiber optic cable positioned to receive light from the anode and vice versa.

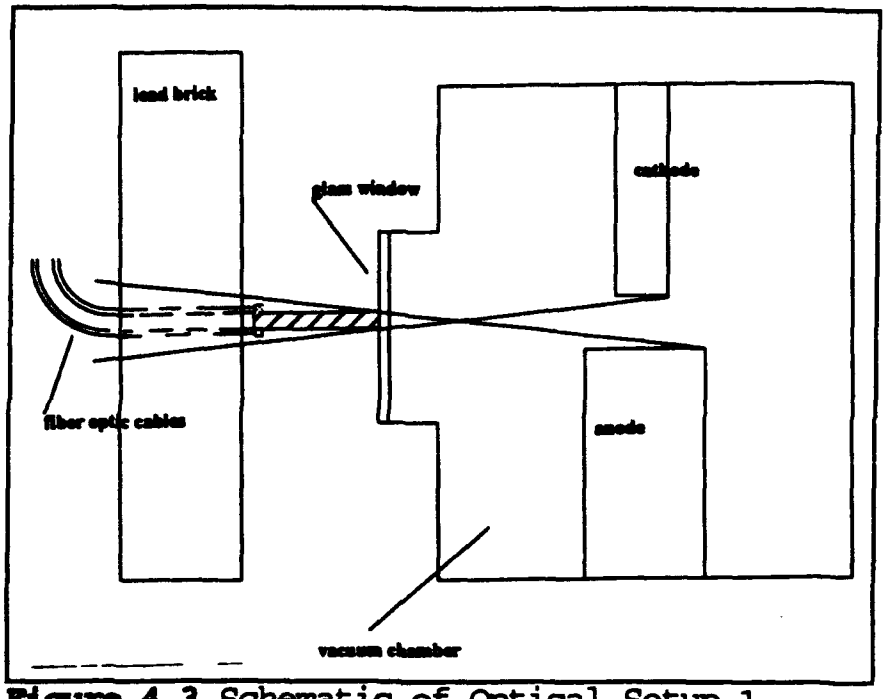

Figure 4.3 Schematic of Optical Setup 1

4. Optical Setup 2

To avoid alignment and reflection problems that could arise in setup 1, an even more stringent method was used to distinguish light sources. It involved the placement of an opaque nonconducting (poly vinyl chloride) disk between the two electrodes. The disk fit snugly inside the vacuum chamber and had a hole in it slightly larger than the anode and cathode diameters. The tantalum foil anode was replaced by a stainless steel bar exactly the same size and shape as the cathode bar. In this way geometrical symmetry was achieved. The PVC disk was centered between the electrodes and parallel to their facing surfaces. The fiber optic bundles were fed through lead bricks as in setup 1 and pointed straight forward on either side of the disk so that light produced on one

electrode would be effectively blocked by the disk from observation by the wrong detector. A schematic is shown in Figure 4.4.

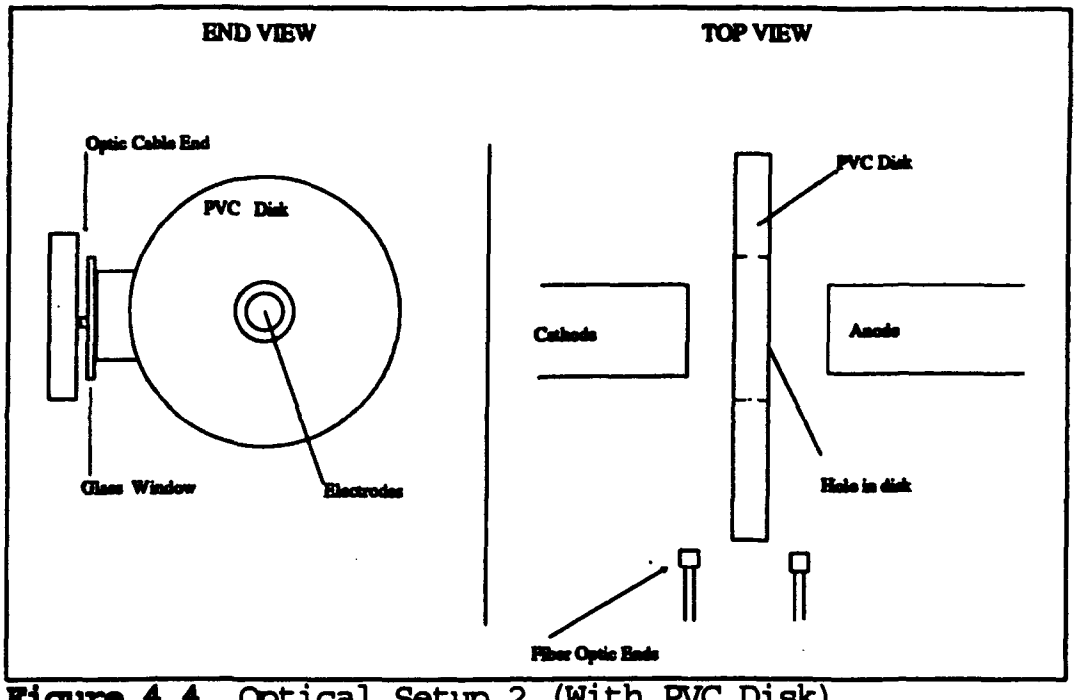

Figure 4.4 Optical Setup 2 (With PVC Disk)

5. X-ray Setup

X-ray signal detection and measurement was the one procedure that had not been done in previous plasma formation experiments and the NPS FXR facility. Finding the right detection equipment required consultation with some detector "experts", and considerable trial and error. Scintillation type detectors were considered, but ruled out due to difficulties in eliminating extraneous signals. Consultations with Mr. George Berzins at Los Alamos National Laboratory, and Mr. Ray Muller at Hammamatsu Corp. indicated that a biased PIN photodiode could be used if we were interested only in the time resolution, and not dose or frequency information. After trying a few detectors, the Lasermetrics Series 3117 Type I silicone photodiode with a 0.4 ns rise time was selected as the most cost effective solution.

Previous experiments at the FXR by Pietruszka [Ref.15] and Galarowicz [Ref.8] indicated placement of the detector along the axis of the FXR for optimal signal reception. The detector was shielded with household aluminum foil to keep out visible light, and reduce electromagnetic noise. Final diode positioning was then determined by taking a series of shots at different distances and voltages to get the optimal signal to noise ratio without saturating the detector. In the operating range of the detector, the signal size was found to be proportional to the radiation dose received, so comparing

relative magnitudes of the signals was possible. The Marx voltages selected for the experiment; 55 kV, 75 kV and 100 kV required the detector to be placed at 5 in. (12.7 cm), 11 in. (27.9 cm), and 31 in. (78.7 cm) respectively from the end plate of the FXR. Doses at 75 kV and 100 kV were also reduced by the use of a 1/2 inch (1.27 cm) lead shield with a 1/2 inch (1.27 cm) aperture along the axis of the diode. This was done to avoid detector saturation. The detector was aligned with the diode axis using the marked geometric center of the diode and a straight steel rod. Because of the collimation involved by the aperture, variations of a few millimeters off the axis of the diode were unimportant especially since we were obtaining only timing information from the signal. Figure 4.5 shows a side view of the X-ray detection setup at the diode end of the FXR.

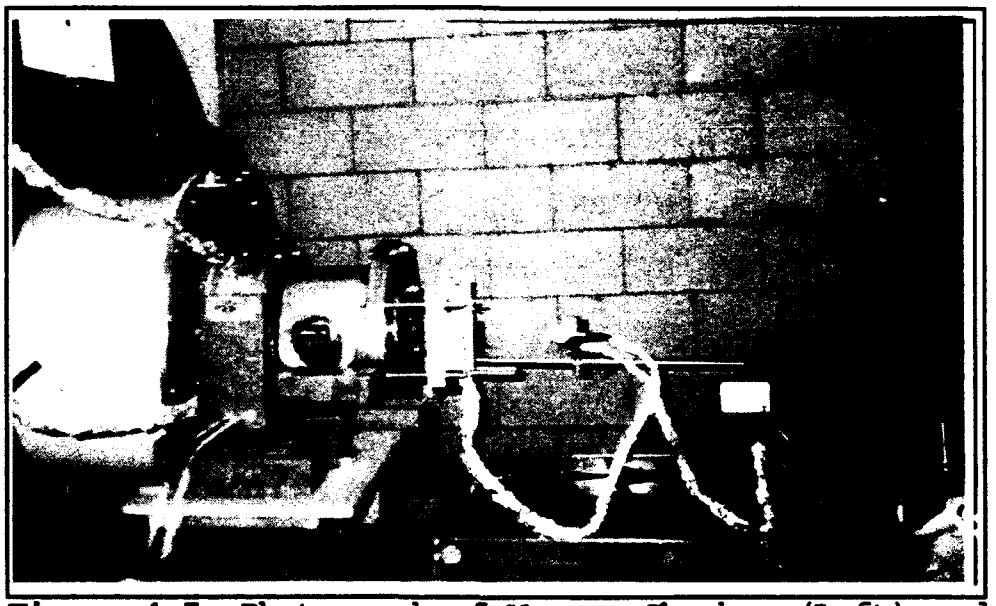

Figure 4.5 Photograph of Vacuum Chamber (Left) and X-ray Detector Setup (Right)

C. PROCEDURES

1. Timing

Ensuring that all of the recorded waveforms were synchronized was a crucial part of the data collection effort. Our method of synchronization compensated for all time differences in the transmission line - oscilloscope systems to include time base and response time characteristics of the oscilloscopes and the length and impedance differences of the transmission cables. To do this we used a Hewlett Packard pulse generator to send a 20 ns pulse down the transmission cables of two of the measuring devices (eg. x-ray and light) simultaneously. We then compared the recorded onset times of the pulse and adjusted the delay generator so that they occurred at the same time (within 0.3 ns). Because we could synchronize only two transmission line - oscilloscope systems at one time, we established the x-ray - DSA system as the base system and synchronized the other three to it. In this way they were all synchronized to each other. We chose the x-ray line - DSA system as the base because it has the shortest cable length, hence its delay could remain zero and synchronization could be accomplished by adding delays to the other systems. We performed our timing in the following manner:

<u>In the Diode Room</u>

1. Attach two coaxial cables of the same length to a "T" connector and attach the "T" connector to the output BNC connector of the pulse generator.

2. Attach one end of a cable to the trigger output of the pulse generator and the other end to an unused twisted coaxial cable.

3. Put following settings on the pulse generator: Pulse width - 20 ns, mode - manual trigger, attenuation - 5dB, trigger advance - 140 ns, wave shape - square.

4. Attach one of the signal output cables to the x-ray detector cable, and attach the other output cables to the cable of the system you wish to synchronize (i.e. voltage, current or light detector cables). Note; you must remove the attenuators from the voltage and current cables first or the signal will be too small.

In the RF Protected Cage

5. Remove the Marx charge line from the trigger input connector of the Delay generator and replace it with the other end of the coaxial cable mentioned in step 2.

6. Ensure oscilloscope/waveform digitizers(DSAs) are set to 1 V/div, 10 ns/div and external trigger. Then put the DCS in the acquire mode.

7. Set all delays to zero on the delay generator.

8. Manually trigger the pulse generator and compare and record onset times of the acquired waveforms. Note, disregard waveforms with ambiguous onset times.

9. Adjust the delay generator corresponding to system being synchronized to match the difference recorded in Step 8.

10. Trigger the pulse generator again and compare onset times. If the difference is less than 0.3 ns, the two systems are considered to be synchronized. Change cable connections and repeat steps 8 and 9 to synchronize another system. If the difference in the onset times is greater than 0.3 ns, adjust the delay generator half the difference and repeat steps 8, 9 and 10 until the difference is less than .3ns.

After completing these steps all cable - scope systems are accurately synchronized but you must add 25 ns (55 kV shots) and 125 ns (75 kV and 100 kV shots) to all of the systems on the delay generator to ensure the waveforms appear on the screen when triggered by the Marx voltage signal. In addition you must apply the following timing corrections to account for transit times of the light and x-rays.

2. Optical Delay Corrections

To compensate for the transit time of the light signal from the plasma in the diode chamber to the photodetectors an optical delay correction must be applied. The light produced on the electrodes must travel a distance, d , of 6 inches(15.2 cm) in the vacuum chamber (index of refraction = 1) to the window (transit time through the window is negligible) and an additional 3 inches (7.63 cm) in air(n = 1) beyond that to the end of the 6 foot (183 cm) long fiber optic cable which has an index of refraction of n = 1.62. Using the relation t = dn/c,

where c is the speed of light, for the two mediums yields a correction of t = 10.7 ns. This delay must be added to the delay generator for the light system.

3. X-ray Delay Corrections

X-rays produced on the anode must travel to the x-ray detector located a certain distance behind the anode. The position varied between 1 and 3 feet depending on the magnitude of the voltage shot being measured. This resulted in x-ray delay corrections between 1 and 3 nanoseconds.

4. Data Acquisition

To obtain the desired waveforms, the Marx Bank capacitors must be charged in parallel and released in series across the diode gap. To ensure this is done properly, the following checklist should be used.

1. Reconnect all cables and attenuators that were disconnected during the timing process.

2. Turn on and properly bias the photo and x-ray detectors.

3. Reset the voltage levels on the oscilloscopes/DSAs and put them in the acquire mode.

4. Set the pressures on the control switches in accordance with the pressure chart.

5. Charge the Marx Bank by turning on all power switches, turning the keys and depressing the charge buttons.

7. Once the Marx Bank is charged to the voltage you have preselected, the ready light will come on. Press the trigger

button and the voltage will be released across the diode. All wave forms will appear on the oscilloscopes/DSAs. For this experiment, one set of ten shots was done at each of three different voltages; 55 kV, 75 kV, and 100 kV (Marx Bank Charge). These charging voltages correspond to approximate peak diode voltages of .6 MV, 1 MV and 1.2 MV respectively. Averages were taken on the ten shots to determine onset times. Additionally one shot was fired with opaque black tape covering the fiber optic cable ends and lead bricks shielding the x-ray detector at each Marx voltage to measure the noise generated in the photo and x-ray detectors. We will refer to these shots as "Blackout" shots from now on.

D. EXPERIMENTAL CONCERNS

1. Electromagnetic Noise

As with previous experiments at the NPS FXR, electromagnetic noise proved to be a troublesome problem to overcome. By using many of the techniques mentioned in previous work [Ref.3,4], such as extensive use of aluminum foil for RF shielding and the placement of the photodetectors as far away from the vacuum chamber as possible, the noise problem became manageable. Another successful improvement we made to the system configuration was to attenuate the relatively high voltage signals (diode and Marx voltages) at the source rather than at the oscilloscope. This reduced the amount of noise pickup in the transmission lines of the photo

and x-ray detectors. The aluminum barrel housing used for the photodetectors also helped reduce E&M noise though it was more effective in attenuating x-rays.

2. Stray X-rays

As discussed earlier X radiation can produce a large signal on silicon diode photodetectors designed to measure visible light. Even with the photodetectors more than six feet away from the vacuum chamber, x-rays produced a sizable signal on the photodetectors. To Block the x-rays from reaching the detectors, we stacked two inch thick lead bricks in front of the detectors. Surprisingly this only slightly alleviated our problem. Through trial and error we found it necessary to block the x-rays from irradiating the fiber optic cables which have a metallic casing. This was accomplished by laying the cables in a lead tray and shielding on the sides with lead bricks.

3. Cathode vs Anode Light

A major concern in this experiment is that of discerning where the light is produced. That is, having confidence that the light produced at one electrode registers only in the detector meant for that electrode. This proved very difficult, because of the vacuum chamber geometry. Many methods were attempted including the lens method similar to that used in [Refs.3,4] but intuitively and through experiment this proved unacceptable. A promising method of employing thin slits in a thick opaque material to limit the field of

view of the detectors, proved unacceptable because the resultant light signals were too small to confidently determine onset times. The divider method described in optical setup 1, if aligned properly, successfully prohibits direct observation of the wrong electrode flares, but probably does allow substantial reflected light from one electrode to enter the other detector. Optical setup 2, with the PVC disk inserted between the electrodes, makes inadvertent direct observation of the wrong electrode nearly impossible and reduces the amount of reflected light to a minimum. However the disk is intrusive to the vacuum chamber where the plasma is formed and could influence the observed phenomena.

V. RESULTS/DATA

A. OVERVIEW

As mentioned earlier, two setups were employed in an effort to effectively differentiate the anode and cathode light sources. The first method (setup 1) using an external separating plate for the two fiber optic bundles proved unsuccessful in this respect. Of the scores of data runs taken using this setup, only a few showed what appeared to be minute differences in onset times for the anode and the cathode light. At the time, we believed this meant that the actual differences in onsets were less than one nanosecond. However after taking data with setup 2, and consistently measuring not only onset time differences but large intensity differences in the light produced, we feel that setup 1 did not perform as designed. Nevertheless the data taken using setup 1 is valuable, because it still accurately records light signal onset which can be compared to the other important parameters measured in the experiment. Callahan, provides an excellent analysis of this data in his work [Ref.16]. Here only the voltage and light waveforms will be analyzed.

The results recorded in this chapter are listed separately by which setup was employed. A special section has also been included to discuss some unexpected phenomena which could be

of interest to planar diode physics but are not believed to have direct consequence on the focus of this paper.

B. TYPICAL WAVE FORMS (SET UP 1)

Ten data runs and one blackout (black tape covering the fiber optic cable ends) run were taken for each Marx bank voltage, 55 kV, 75 kV and 100 kv voltages. Diode voltage, light, and blackout signals are shown below in figures 5.1 through 5.9. Light signals in these figures are deliberately not labelled anode and cathode so as not to be misleading, because it is not believed that the setup adequately distinguished the two light sources.

55 kV Marx Voltage Shots

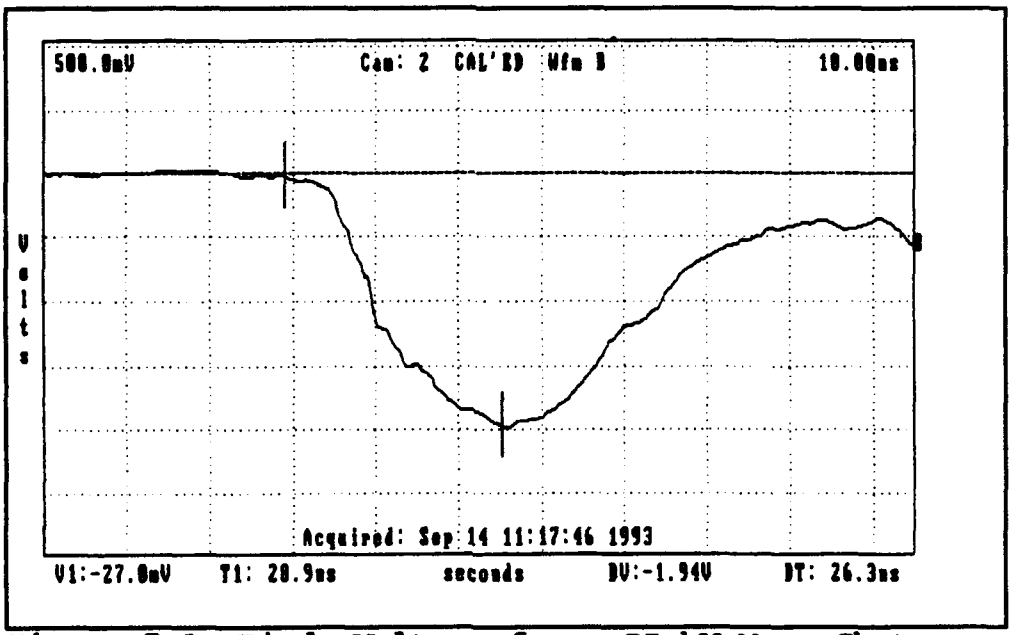

Figure 5.1 Diode Voltage for a 55 kV Marx Shot. Onset is denoted by the left tick mark at 29 ns.

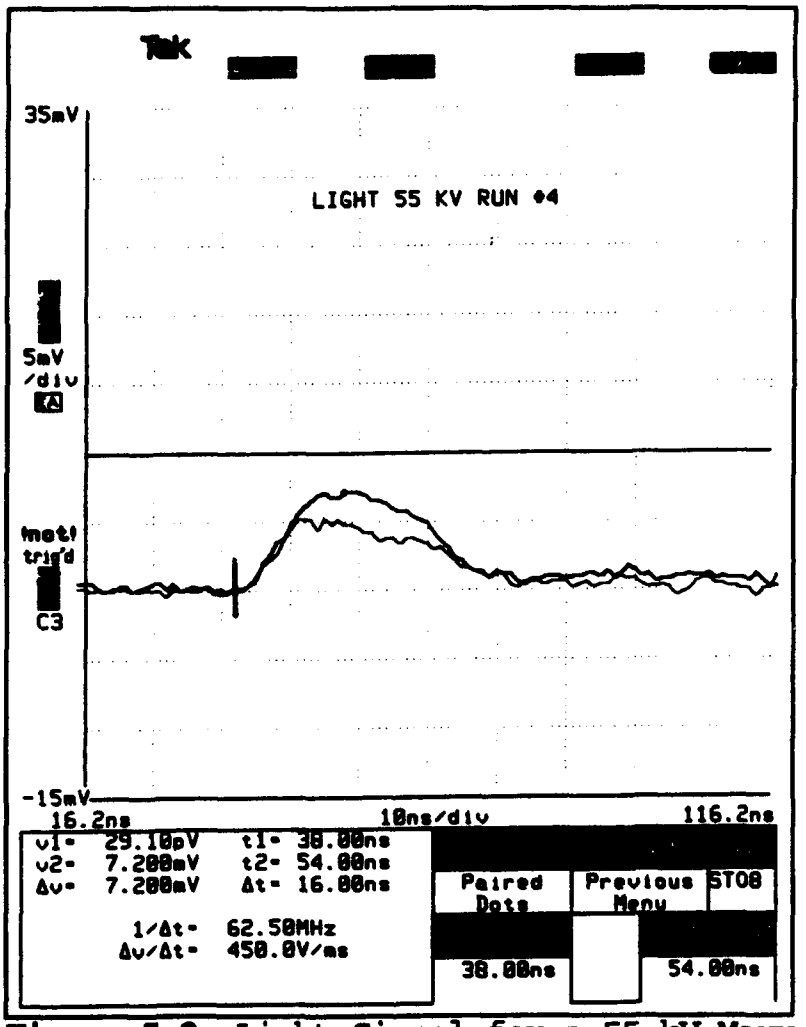

Figure 5.2 Light Signal for a 55 kV Marx Shot. Onset times for both anode and cathode signals is 38 ns.

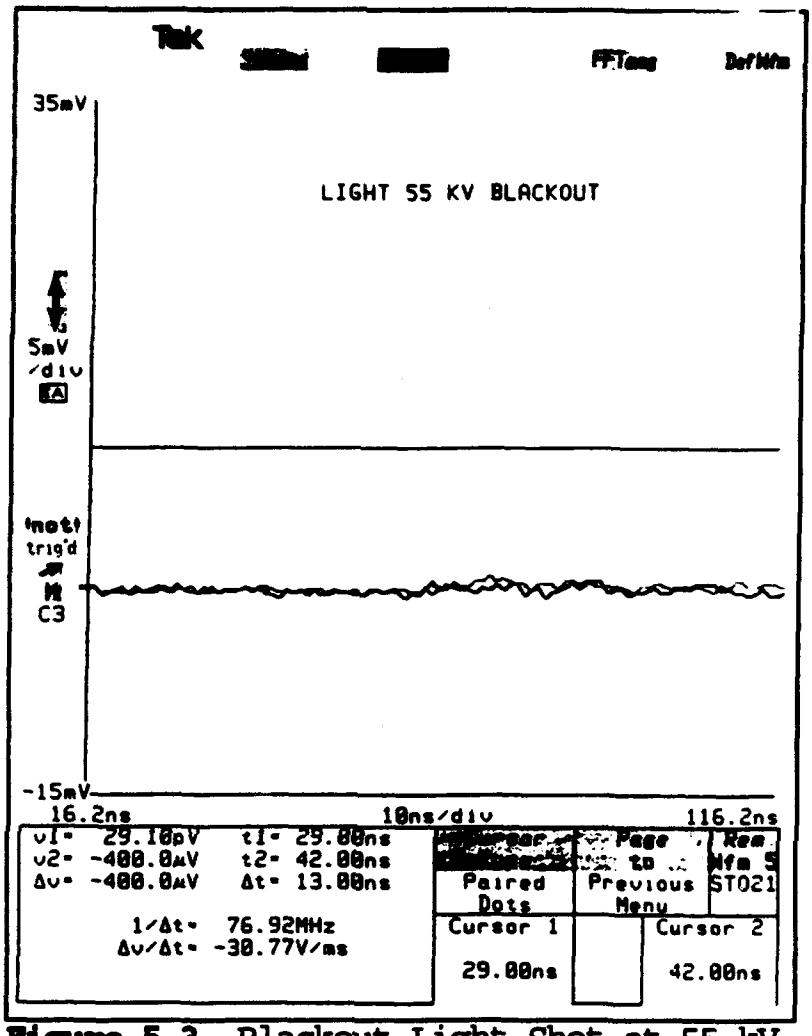

Figure 5.3 Blackout Light Shot at 55 kV Marx Voltage. Fiber optic cable ends were covered with black tape.

For the 55 kv Marx run shown in Figures 5.1-5.3, the onset times for the light signals occur 9 nanoseconds after the voltage onset. The two light signals are relatively small, but definitely distinguishable above the very small background noise.

75 kV Marx Voltage Shots

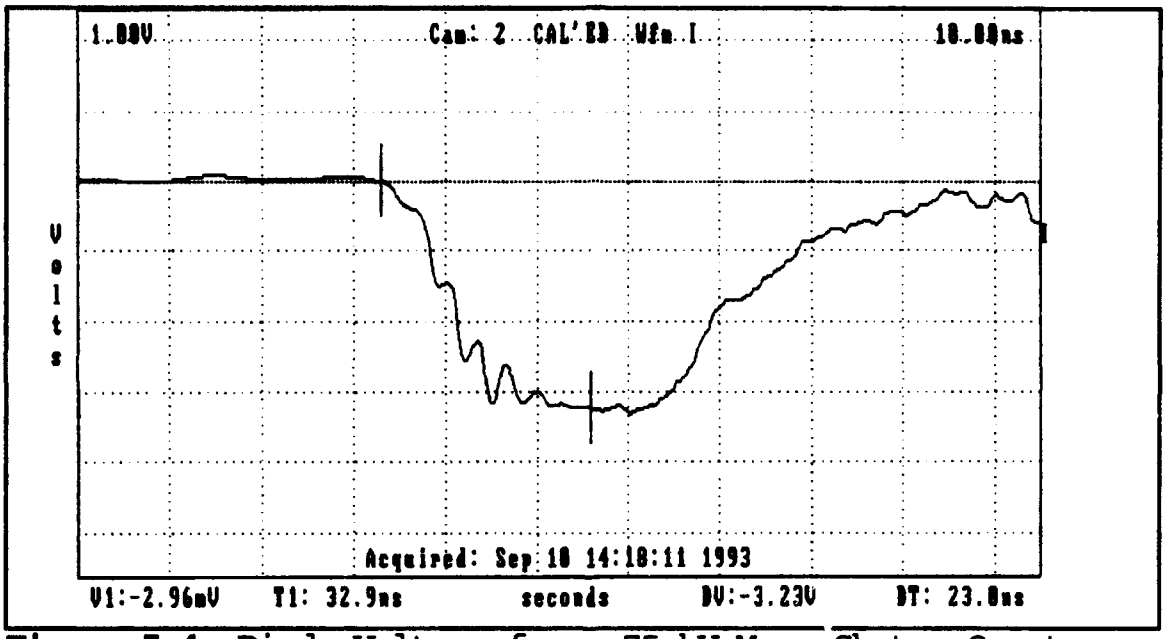

Figure 5.4 Diode Voltage for ϵ 75 kV Marx Shot. Onset occurs at 33 ns.

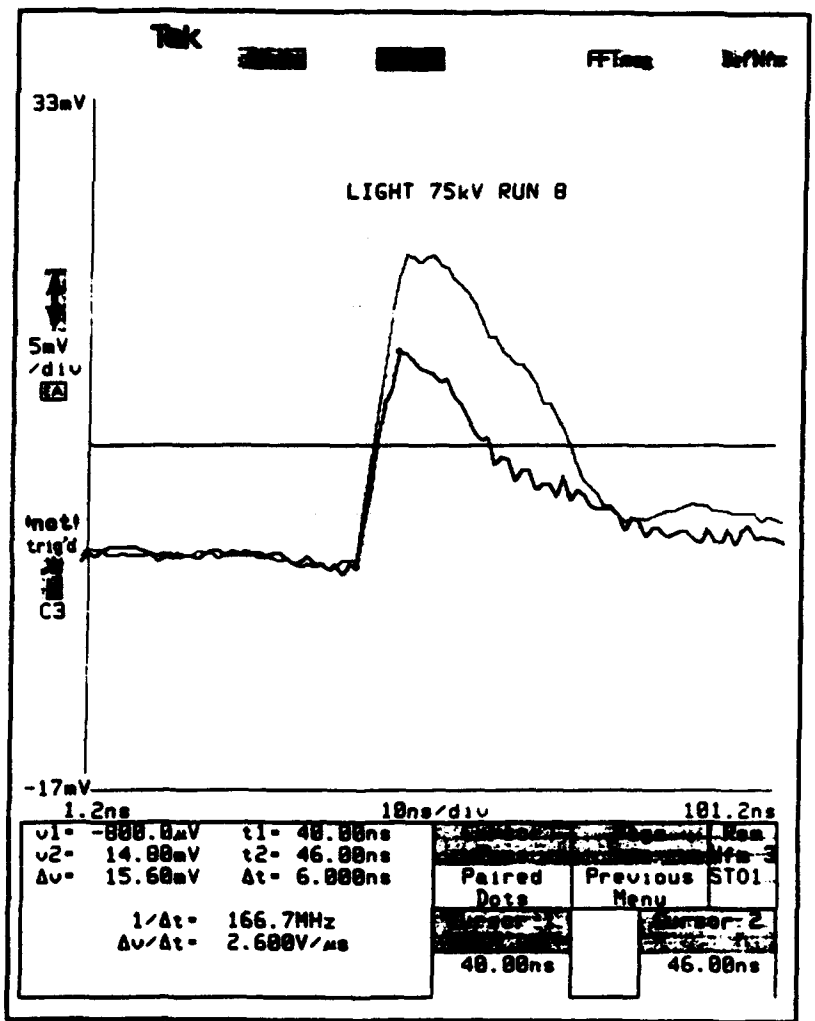

Figure 5.5 Light Signal for a 75 kV Marx Shot. Both onsets are at 40 ns.

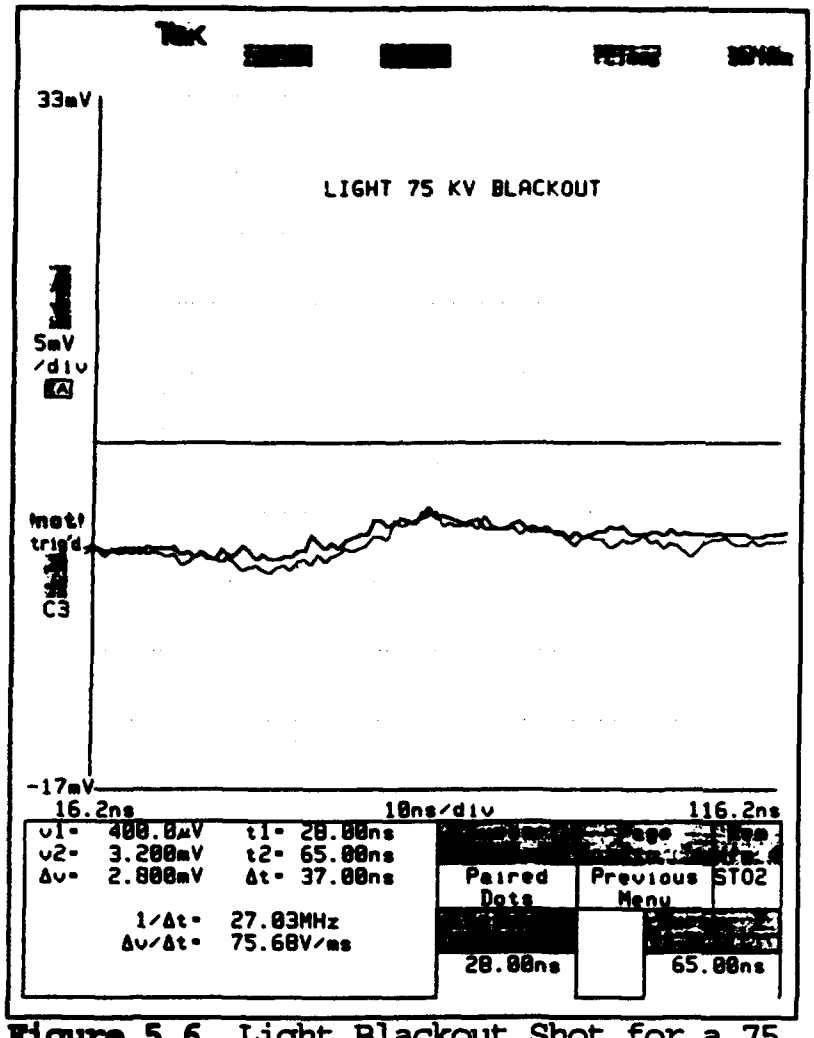

Figure 5.6 Light Blackout Shot for a 75 kV Marx Voltage. The slow noise rise begins at 47 ns and peaks at 64 ns.

The difference in onset times for the 75 kV run, shown in Figures 5.4-5.6, is 7 ns. The background noise is larger than for the 55 kV runs. This is probably attributable to stray x-rays registering in the photodetectors, but could be electromagnetic noise. However, the slow rise that appears in the blackout signals always occurs after the light onset so the noise rise cannot be mistaken as light onset.

100 kV Marx Voltage Run

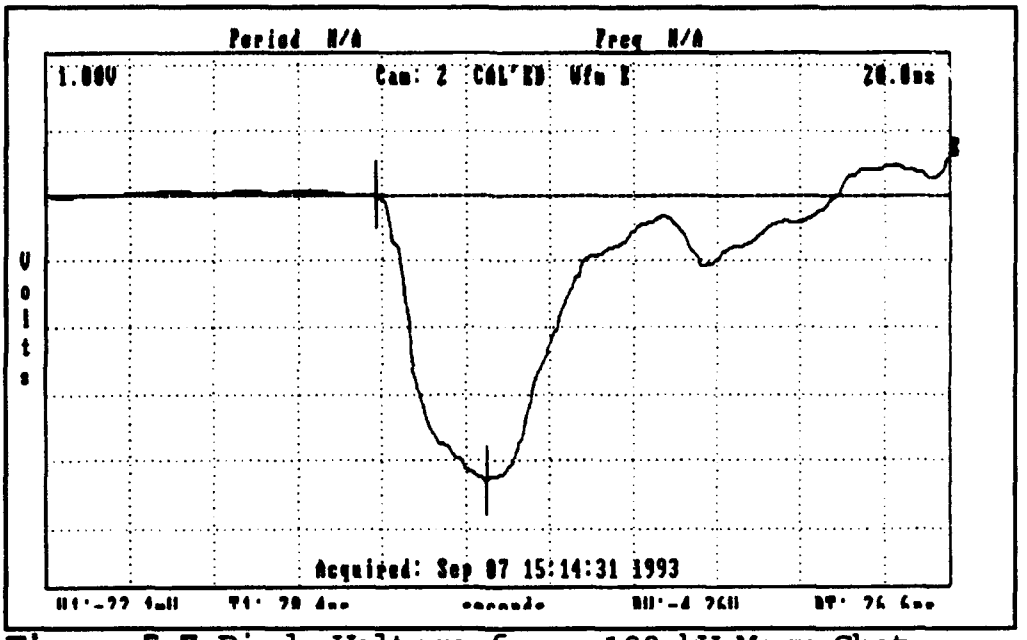

Figure 5.7 Diode Voltage for a 100 kV Marx Shot. Onset is at 78 ns.

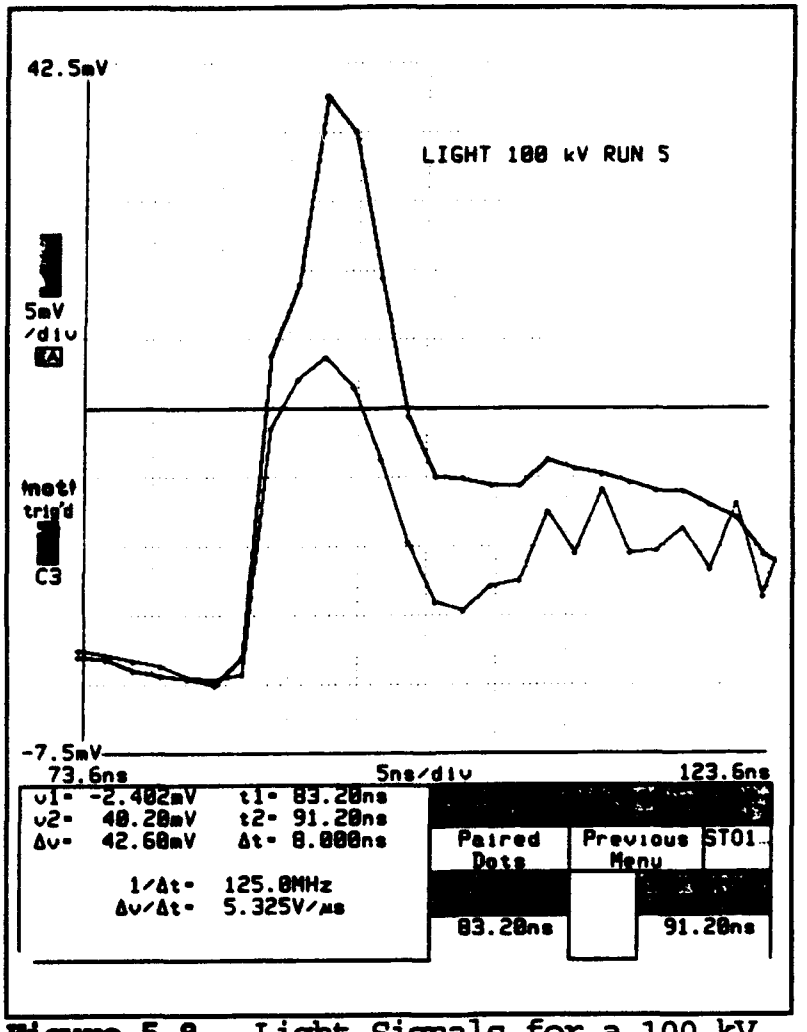

Figure 5.8 Light Signals for a 100 kV Marx Shot. Onset occurs at 83 ns for the "anode" signal and 85 ns for the "cathode" signal.

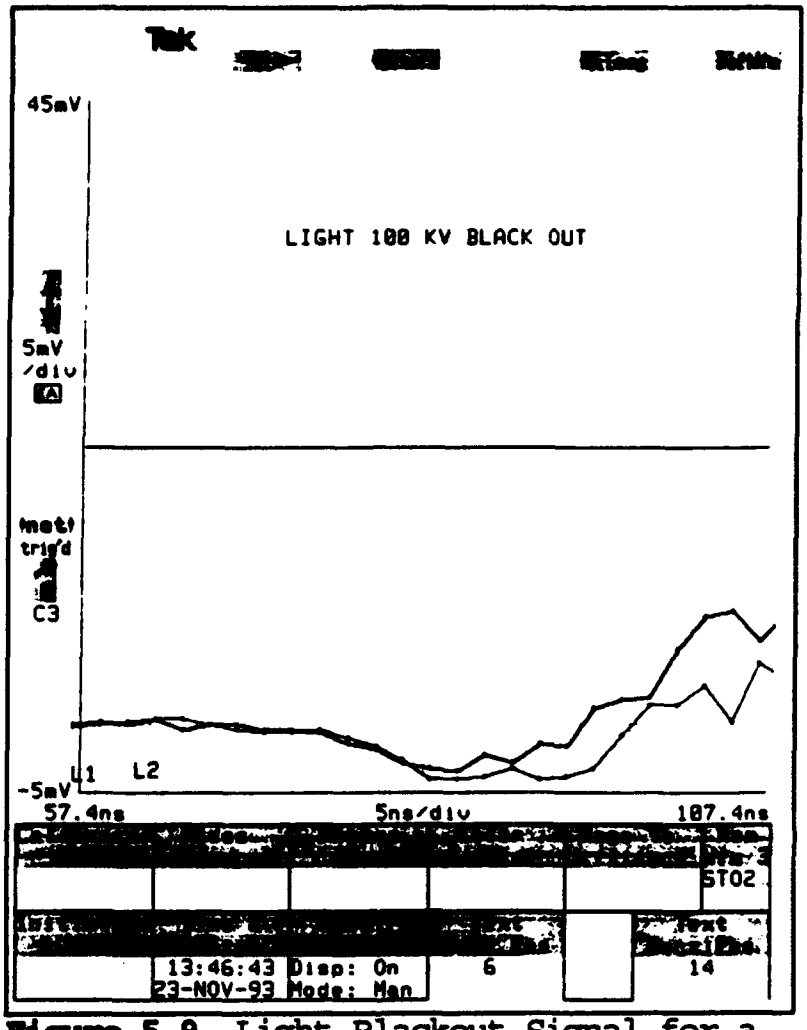

Figure 5.9 Light Blackout Signal for a 100 kV Shot. Pull down begins at 74 ns. Rise after pull down starts at 89 ns.

For this 100 kV Marx voltage shot, shown in Figures 5.6-5.9, the difference in onsets is 5 ns. The blackout signal is not small but as with the 75 kV shots, the rise after the pull down occurs well after the onset of the light and therefore will not affect the perceived location of light onset.

C. TABULATED DATA (SET UP 1)

All onset times and other values listed below were determined by magnifying the signal with the zoom feature on the DCS or the magnify features on the DSA. Averaged values of important parameters for a ten run sequence are listed in tables 5.1 and 5.2 below.

Table 5.1 AVERAGE ONSET TIME DIFFERENCES FOR SETUP 1

Marx	(light onsets) Anode vs Cathode	Cathode Light vs Diode Voltage	Timing Error
55 kV	-0.1 ns *	10.33 ns	±1.2 ns
75 kV	+0.1 ns *	6.58 ns	±1.2 ns
100 kV	-0.1 ns *	5.86 ns	±1.2 ns

*The " + " indicates cathode onset before anode onset

The onset times for the anode and cathode light were the same for every data run except one in each group of ten trials, hence the 0.1 ns average difference. The light and voltage onset time differences became smaller with the higher Marx voltages.

Table 5.2 DIODE VOLTAGES AT LIGHT ONSET AND LIGHT INTENSITY RATIOS FOR OPTICAL SETUP 1

Marx	Diode Voltage @ Light onset	Voltage Error	Light Intensity Ratios Cath./Anode
55 kV	401 kV	±54 kV	0.86
75 kV	441 kV	±125 kV	0.67
100 kV	304 kV	±230 kV	0.58

All of the applied voltages, Φ , in Table 5.2, correspond to macroscopic electric fields greater than the estimated 10^7 V/m needed for field emission to occur. Using this setup, the anode light signal was always slightly larger than the cathode signal. This was probably due to minor detector and coupling differences. The signals should be about the same because the detectors in this setup were for the most part "seeing" the same light. For this same reason the differences in onset of anode-cathode light could not be distinguished using setup 1. Calculations for the voltage error shown above are contained in Appendix B.

D. TYPICAL WAVE FORMS (SET UP 2)

With this setup, in which a disk was inserted between the anode and cathode, the light signals could be distinguished. Three very important characteristics can be seen from the Figures 5.10 - 5.12 below: 1) There is always a discernible difference in onset times between cathode and anode light and 2) the cathode light signal starts with a slow rise for 1-2 ns and is followed by a sharp rise, and 3) The cathode light signal is much larger than the anode light signal except for the 85 kV and 100 kV shots. Interpretation of these characteristics is described in the Analysis Chapter of this Work. The data runs were all accomplished in one day in the following order: 75 kV Marx, 100 kV Marx, 55 kV Marx, and 85 kV Marx.

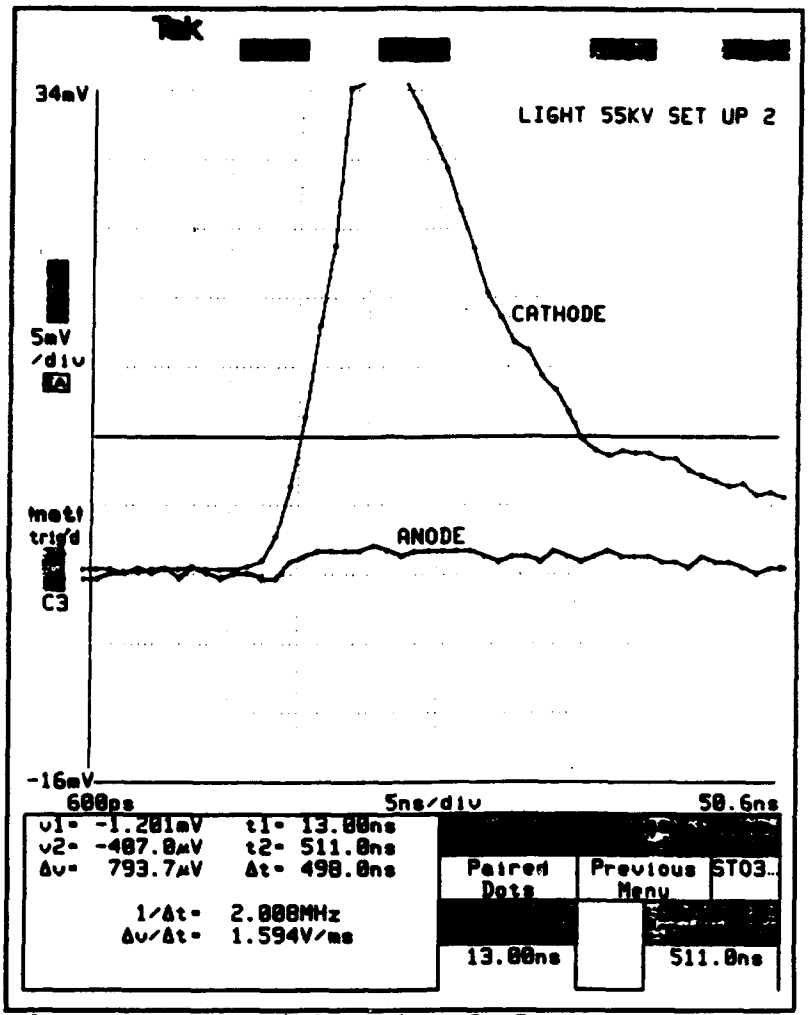

Figure 5.10 Light Signal for a 55 kV Marx Shot (With PVC Disk). Cathode light onset is at 12 ns. Cathode Ramp :13 ns. Anode onset 14 ns. Cathode peak: 171 mV.

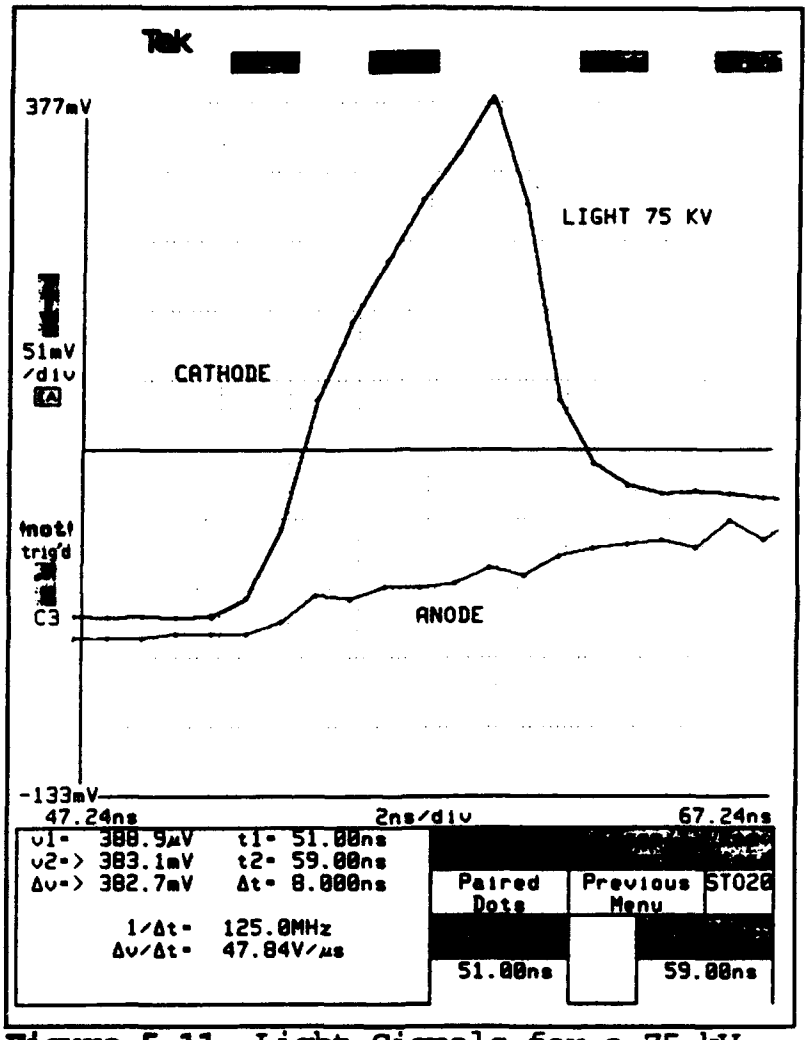

Figure 5.11 Light Signals for a 75 kV Marx Shot. Cathode onset is at 60 ns. Cathode Ramp: 61 ns and anode onset:62 ns. Cathode peak: 386mV, anode peak: 27mV

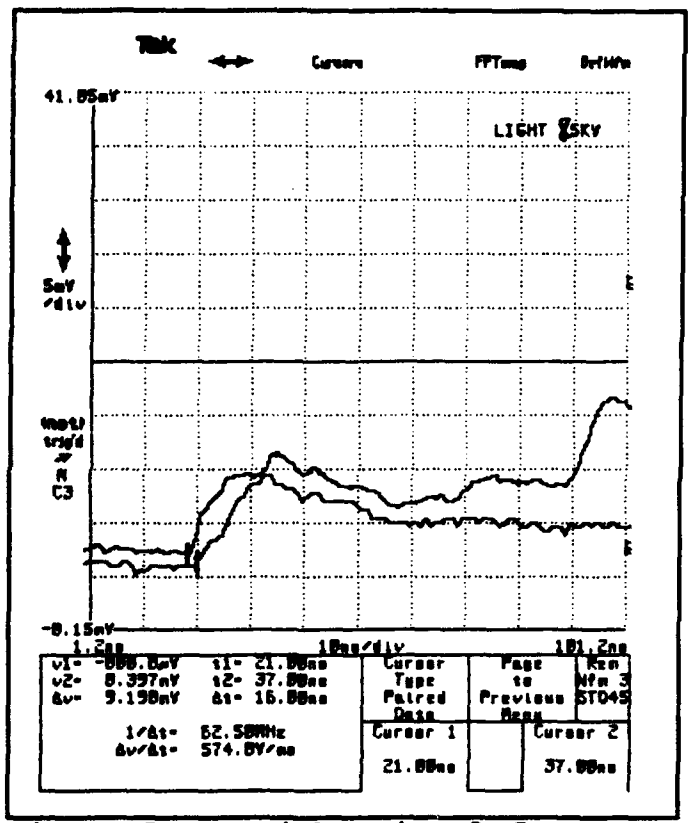

Figure 5.12 Light Signal for an 85 kV Marx Shot. Cathode light onset occurs 1 ns before anode light onset.

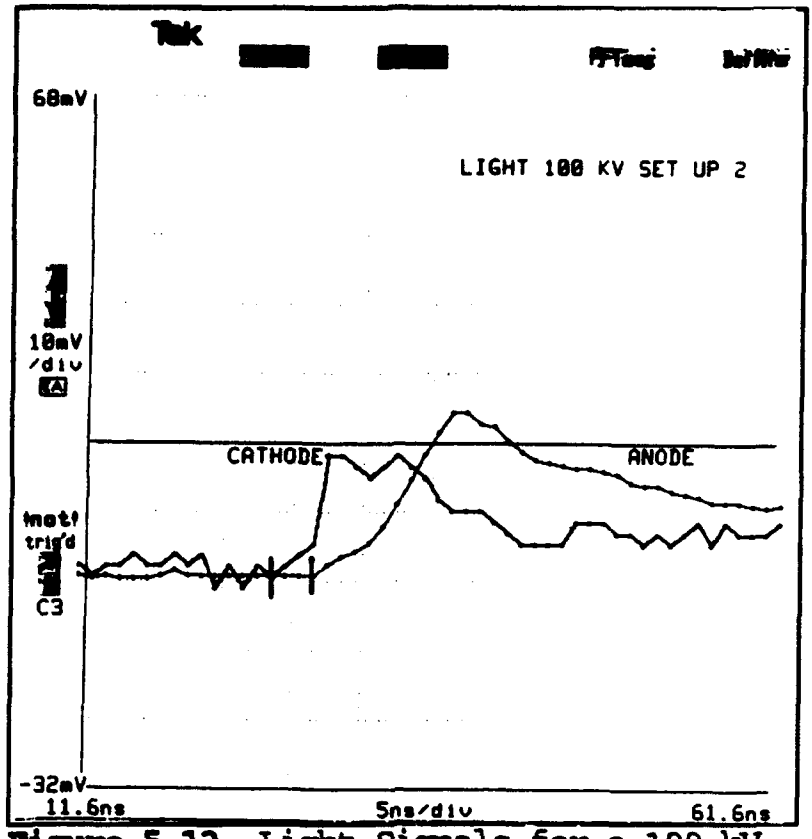

Figure 5.13 Light Signals for a 100 kV Shot. Cathode onset begins at 25 ns and ramps at 28 ns. Anode onset is at 28 ns.

E. TABULATED DATA (SET UP 2)

Light onset time differences between the two electrodes were averaged for each Marx voltage. This difference did not vary much based on Marx voltage. This information is listed in table 5.3. Unlike the case of setup 1, in setup 2 (with disk) the intensity of the light produced at the anode and cathode were significantly different for the 55 kV and 75 kV runs. In these cases the cathode light signals are much

greater than the anode signals. This information is listed in Table 5.4.

Table 5.3 LIGHT ONSET TIME COMPARISONS FOR SETUP 2

Marx	Onsets Cath vs anode	Std Dev	Onsets Anode vs Cath.Ramp
55 kv	1.4 ns	0.55 ns	0.2 ns
75 Kv	1.25 ns	0.75 ns	.083 ns
85 kv	1.5 ns	0.71 ns	N/A
100 kv	2.5 ns	0.71 ns	0

The data in Table 5.3 shows that the anode light begins 1.4 ns after the cathode light for a Marx charging voltage of 55 kV, 1.25 ns for a 75 kV Marx voltage, 1.5 ns for an 85 kV Marx shot and 2.5 ns for a 100 kV Marx shot. However, the anode light begins almost simultaneously with the cathode fast rise

ramp, which we associate with the ionization of the neutrals in front of the cathode. This is explained in further detail in the Analysis Chapter.

Table 5.4 AVERAGE LIGHT SIGNALS AND RATIOS

Marx	Average peaks Cathode	Anode	Ratio Cathode/Anode
55 kV	62.6 mV	1.94 mV	32
75 kV	321 mV	14.8 mV	22
85 kV	5 mV	7 mV	0.7
100 kv	11.7 mV	22.6 mV	0.5

Both light signals appear to be suppressed for the 85 kV and 100 kV runs. The magnitude of the anode light signal is greater than the cathode signals for these runs also. For reasons explained in the Analysis Chapter, we believe the data from the 55 kV and 100 kV Marx runs to be most representative of typical plasma formation on the electrodes.

F. ADDITIONAL FINDINGS

After obtaining the data using setup 2 (with the PVC disk in the chamber), the electrodes were removed from the vacuum chamber for inspection. What we discovered was very unexpected. The anode had sustained severe damage and lost an unprecedented amount of material. In fact it had a large inverted pyramidal shaped gouge into the surface about .4 cm deep with a .7 cm base. The cathode in turn was plastered with the anodic material that was ripped from the anode. Photographs of the electrode surfaces are shown in Figures 5.14 and 5.15.

In previous work at the NPS FXR, the anode has always sustained very little damage. Typically the cathode sustains most of the material loss, but this damage is orders of magnitude less than the anode damage observed after pulsing the diode with the PVC disk inserted. For comparison, photographs of the tantalum foil used in setup 1 and a stainless steel anode used by Willis [Ref.4] are shown in Figures 5.16 and 5.17. The surfaces show very little damage and are smooth to the touch. Photographs of both sides of the PVC disk are shown in Figures 5.18 and 5.19. The Cathode side of the PVC disk is clearly scorched, while only a very small amount of discoloration is visible on the side facing the anode.

The only changes made to the diode configuration during the time the anode damage occurred were the insertion of the

PVC disk and the replacement of the large area tantalum foil anode with a smaller stainless steel anode. To isolate which change caused the damage to occur, we removed the PVC disk and fired the machine over 40 times at high voltages. No damage to the anode surface like that shown in Figure 5.14 occurred. This indicates that the PVC disk played a role in damaging the anode.

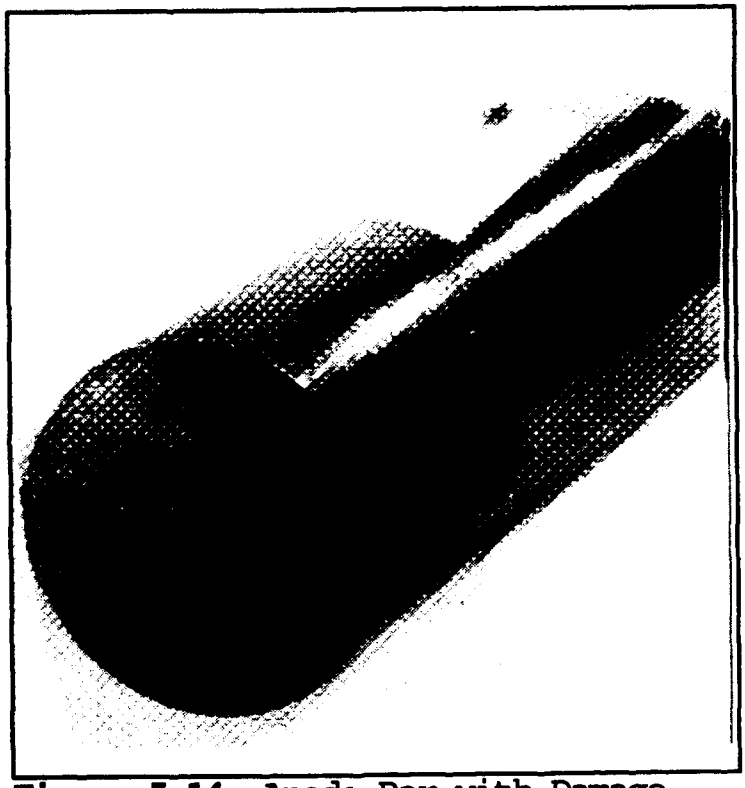

Figure 5.14 Anode Bar with Damage

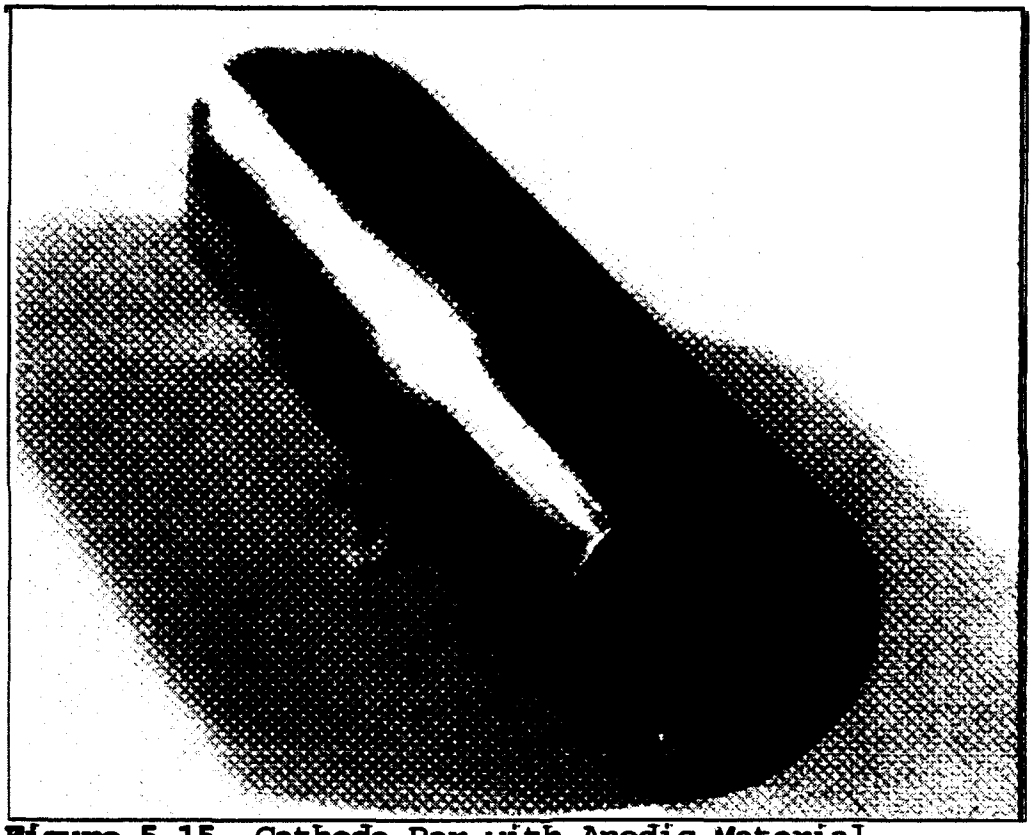

Figure 5.15 Cathode Bar with Anodic Material Plastered on it.

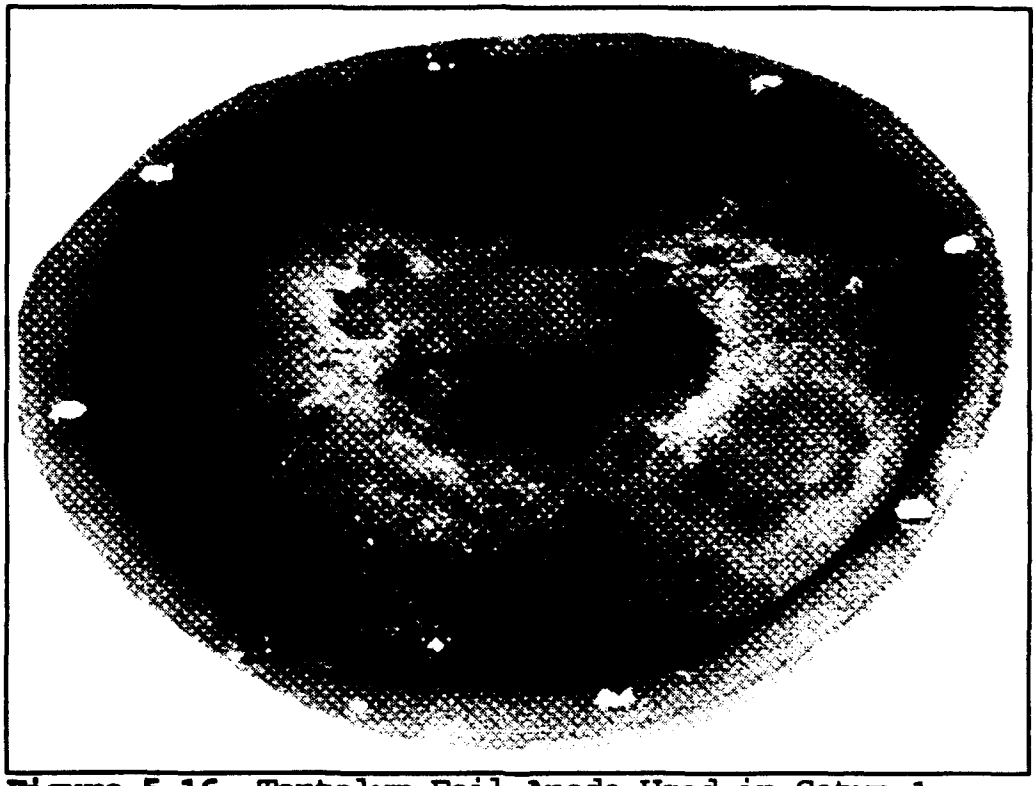

Figure 5.16 Tantalum Foil Anode Used in Setup 1. Very little macroscopic damage. Texture is smooth.

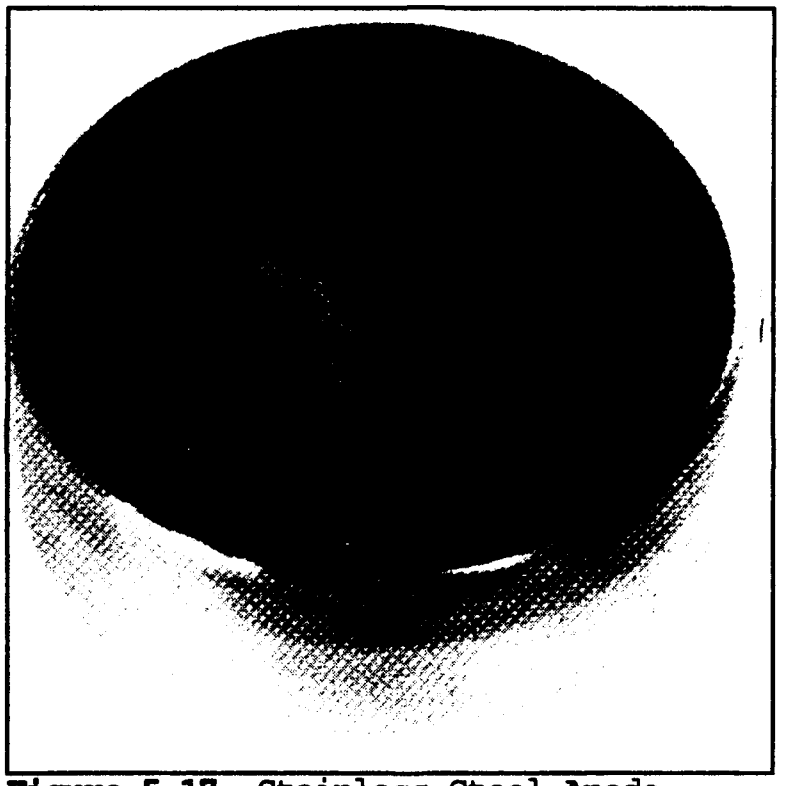

Figure 5.17 Stainless Steel Anode. Surface is only slightly roughened.

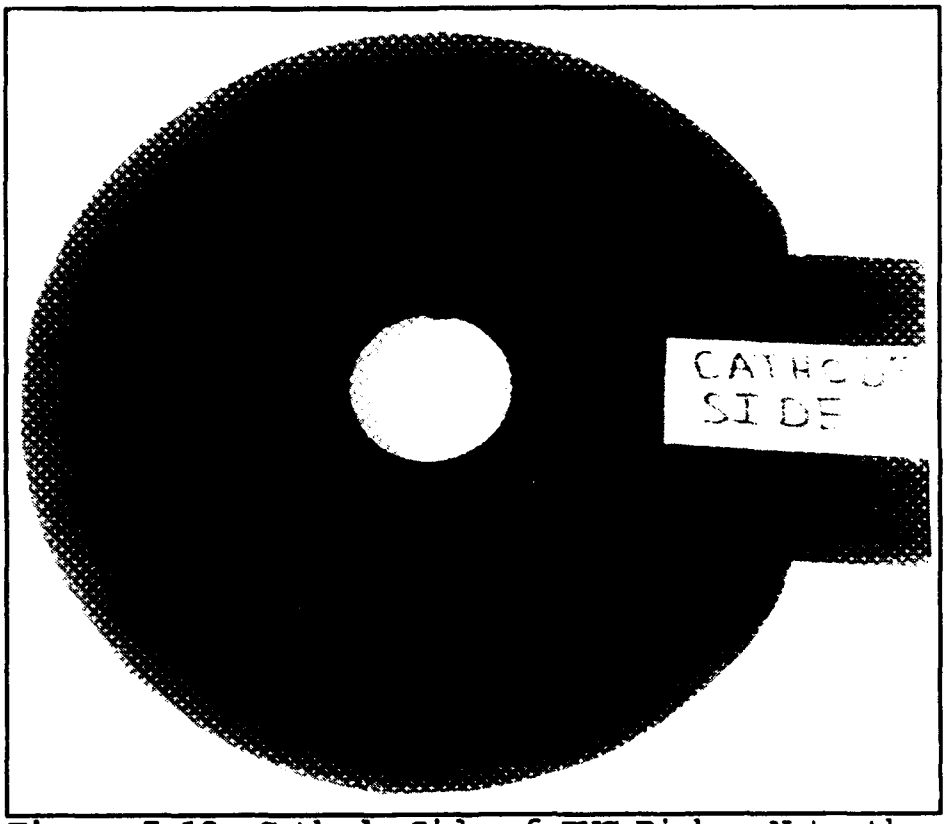

Figure 5.18 Cathode Side of PVC Disk. Note the scorched area of the inner rim.

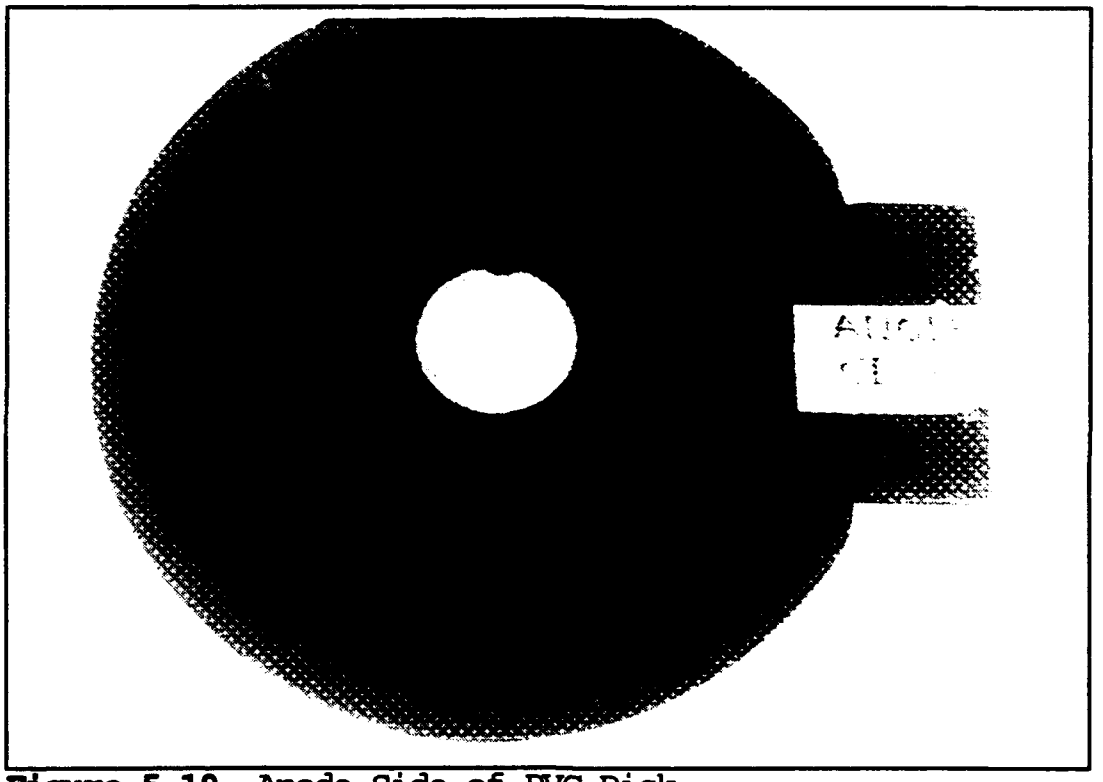

Figure 5.19 Anode Side of PVC Disk.

VI. ANALYSIS

A. OVERVIEW

Experimental results support the Desorbed Neutral Ionization, DNI, model as it applies to both the anode and the cathode in a number of ways. One of the most promising results are the very accurate timing predictions for the onset of cathode light after voltage onset. A table comparing predicted versus experimental results is in the next section. The sequence of events predicted by the model is borne out by measured data. The models covered in the theory chapter describe simplistic versions of what is actually the result of many complex and simultaneous events, but those key measurable events which must occur in order in fact do. Specifically, voltage onset is followed by reaching the 10^7 V/m threshold for field emission which precedes light production on the cathode which precedes light production on the anode. All this is in agreement with the DNI model. Another important finding is that the light produced on the cathode is significantly brighter than that produced on the anode. This is to be expected because the ionic sheaths near the cathode surface is assisted by the applied voltage while the ionic sheath near the anode surface must overcome the applied voltage to set up unipolar arcs.

B. LIGHT ONSET PREDICTIONS

The light signals recorded in optical setup 1 are likely a combination of both anode and cathode light. Their onset times must correspond with that of the earliest light produced. It was discovered in setup 2 that cathode light occurs first. It is therefore assumed that the onset times recorded in setup 1 are in fact the time of the first measurable light produced at the cathode. The time delays between voltage onset and cathode light onset predicted by the DNI model in chapter III are compared to those measured by experiment in Table 6.1 below.

Table 6.1 LIGHT ONSET TIME PREDICTIONS FROM FIGURES 3.4-3.6 VS EXPERIMENTAL MEASUREMENTS.

Marx	Delay times predicted	Delay times measured	Measured error
55 kV	11 ns	10 ns	±1.2 ns
75 kV	7.5 ns	6 ns	±1.2 ns
100 kV	7.5 ns	6 ns	±1.2 ns

The measured values are very close to those predicted by the DNI model. The measured delays are 1 to 1.5 ns less that the predicted values. This is almost within the 1.2 ns timing

error window (see Appendix B for error analysis). It is important that they are shorter than predicted by the model because of the assumptions inherent in the model. One assumption is that the neutrals move away from the cathode with an average speed of 470 m/s. But the velocity distribution of the molecules is gaussian so many molecules will have speeds greater than 470 m/s (and many less), and these molecules will reach the ionizing potential a little earlier. A similar argument must be made for the 100 V maximum of ionization cross section. Though it is not arbitrary, ionization cross sections at slightly less energies say 70 eV are still appreciable and some ionization will occur. So for these reasons it is more likely that experimental delay times be shorter than those predicted.

C. SEQUENCING

The sequence of measured events supports both the EEE and DNI models. But the ramping phenomena on the cathode light pulses is better explained by the DNI model. Our interpretation of the ramp phenomena is that the typical initial slow rise of 1 ns of the cathode signal is the light created by the ionization of the neutral cloud and that the sharp rise or ramp is the resulting cathode flare. This makes sense because the ionization of gas at near atmospheric pressure will produce an easily detectable light signal but should be much less intense than the light from the following

explosive like plasma formation (cathode flare). A time line of events depicting measurements and their corresponding interpretation for a typical 55 kV Marx shot is shown in Figure 6.1.

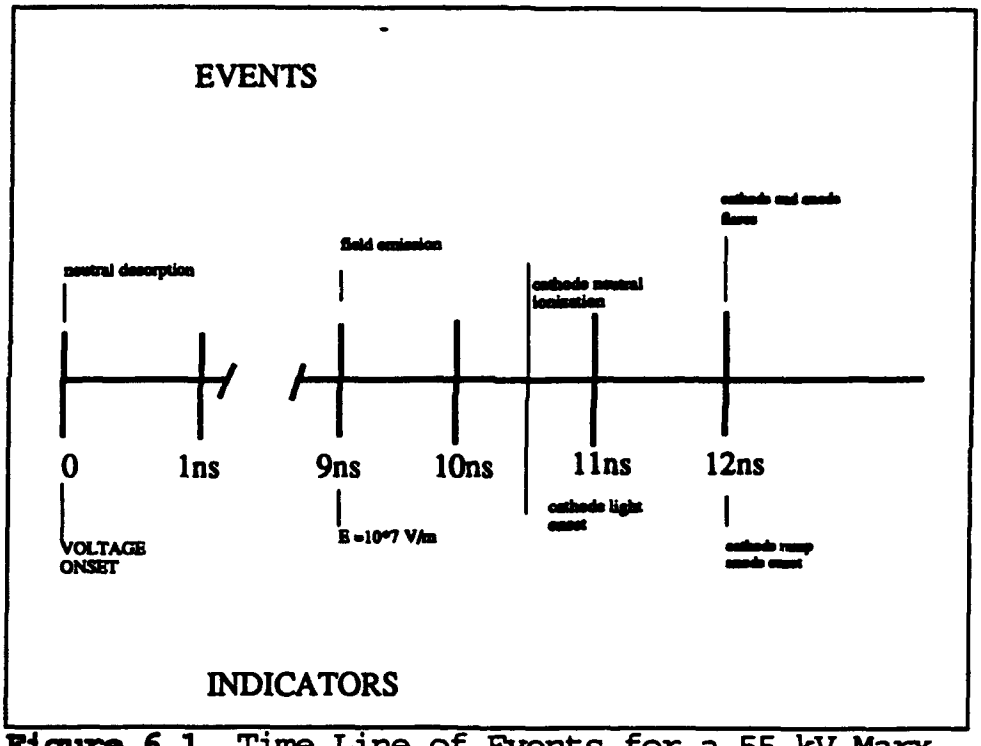

Figure 6.1 Time Line of Events for a 55 kV Marx Shot

It is also important to note that the anode light occurs within the predicted 0-2 ns range after the cathode flare. It can be seen from table 5.1 that the anode light signal onset coincides not with the cathode onset but with the cathode ramp. The conclusion therefore is that anode flares occur

less than 1 nanosecond after cathode flares but 1.5 ns after onset of cathode neutral ionization.

D. LIGHT INTENSITIES AND CRATERING

As mentioned earlier, the light produced at the cathode for the 55 kV and 75 kV Marx shots (Using Setup 2) was much greater (32X and 22 X respectively) than that of the anode. This is not a result of differing detector sensitivity because the detectors were switched for approximately half the shots with the same result. This phenomenon did not occur for the few 85 kV and 100 kV shots. In these shots the anode signal was slightly larger than the cathode signal, but both signals were much smaller than would be expected for these voltages. Past experience with hundreds of shots shows that the light signal actually grows with increased Marx bank voltage. Typical light signal peaks for 100 kV shots with the same detectors and the same fiber optic bundles flush against the window are well over 100 mV. The reason for the loss of light signal is unclear. Subsequent shots taken after removing the disk (and replacing the damaged anode) showed the light signal randomly losing and regaining its intensity for 55 kV, 75 kV and 100 kV Marx Voltages. Probably an insufficient number of data runs were taken at the 85 kV and 100 kV charging voltages. Only two shots each were taken at these voltages because the light output was so low. Persistence at these Marx voltages may have resulted in a regained signal. It's

possible that since both signals were very small and the charging voltage very high that the arcing occurred, not across the diode gap, but to the plastic disk or the walls of the chamber. For these reasons it is believed that the 55 kV and 75 kV data are most representative of typical plasma production on the electrodes.

The greater intensity of the cathode flares can be explained by the fact that cathode flares are produced with the assistance of the applied electric field, while the anode sheath must overcome the applied field. The result should be a reduced number of craters on the anode surface. Using photographs of craters in [Refs.2,4], we estimate cathode spot densities are typically $\approx 10^6$ cm^{-2}, and anode spot densities are about $\approx 10^3$ cm^{-2}. Based solely on spot densities one would expect the cathode light to be 1000 times that of the anode. However plasma production is being observed from the side of the electrode surfaces and it is therefore an *optically thick* medium. That is, much of the light produced on both surfaces is in effect masked by the plasma light lying between it and the detector. More plasma light is produced at the cathode, so the masking effect is greater at the cathode. The optical thickness of the plasma produced in front of the electrodes therefore has an equalizing effect on the two light signals. The DNI model thus provides an explanation for the brighter cathode light while the EEE model incorrectly predicts (at least for our diode conditions) that the anode light will be

greater. The EEE model also does not explain how the dissolution of anode matter occurs in the form of craters but the DNI model, via unipolar arcing, does provide an explanation.

E. ANODE DAMAGE

Since no damage to the new anode was observed after numerous high voltage firings, with the PVC disk removed from the vacuum chamber, it is believed that the disk played some type of focussing role on the high energy electron beam. It is possible that there was a negative electrical charge build up on the rim of the disk hole where the burn marks appear. This was probably caused by bombardment of flux electrons produced by the cathode flares. This is possible because poly vinyl chloride has a very high dielectric strength. The negatively charged rim could then focus follow on electrons to the center by coulomb repulsion. Further investigation is needed, however, to confirm this assumption. It is important to note here that the insertion of the PVC disk most probably did not effect the results recorded for initial plasma production on the electrodes. At the beginning of the application of each voltage pulse the disk is uncharged and therefore invisible to the electrodes. It is not until after the cathode flare has already occurred that the disk is charged and the beam focussed. All of our measurements are taken before this time.

VII. CONCLUSION/RECOMMENDATIONS

The results of this experiment shows the occurrence of three important phenomena that until now had not been observed. The first is that the light signal produced near the cathode surface during the onset electrical breakdown begins before the first measurable light emanating from near the anode. The second is that the light produced near the cathode is much brighter than the light produced near the anode. The third is that the cathode light signal typically begins with a slow rise and is followed within 1-2 ns by a very rapid rise. In addition, measurements of light and diode voltage onset times were made for comparison with predictions published in previous work [Ref.3].

The results of this experiment confirm what has been believed for years, that cathodic processes initiate and dominate plasma production in vacuum diodes. The confirmation comes from both the earlier onset of light coming from the cathode surface and its much greater intensity. Two models predict the dominant role of the cathode in vacuum diode electrical breakdown, the Explosive Electron Emission Model and the Desorbed Neutral Ionization model. The results of this experiment tend to support the DNI model in the following ways. The DNI model's predictions for the time delay between voltage and light onsets are very accurate. The measured delay times were only 1 to 1.5 ns earlier than the predicted

times. These earlier than predicted delays are to be expected because of the assumptions used in the model. The measured sequence of events agrees with those of both the EEE and the DNI models. The often observed initial slow rise of the cathode light signal followed in a couple of nanoseconds by a very steep rise can be explained using the DNI model. It is believed that the slow rise possibly represents the light produced by the neutral molecules being ionized near the cathode surface and that the steep rise is the result of unipolar arcing. The EEE model provides no other comparable explanation for this signal shape. The DNI model also predicts the brighter cathode light that was observed in this experiment, whereas the EEE model predicts the opposite. The EEE model also does not explain the occurrence of craters on the anode surface.

Further work in this area is needed for a more complete understanding of the electrical breakdown process. A spectral analysis of the radiation produced before and during the breakdown process could provide insight into what processes are taking place. This would be especially enlightening if this could be accomplished with temporal resolution. In regards to the unexpected damage to the anode, which could be a result of a focussing effect of the PVC disk, further testing using different materials and geometries should be attempted to maximize the effect. This could potentially be very important in charged particle beam applications.

APPENDIX A: ERROR ANALYSIS

A. TIME MEASUREMENTS

This section explains the timing error calculations used in the results and analysis chapters of this report. The sources of error are divided into two categories. The first being those that are compensated for by the synchronization procedures outlined in the experiment section including time base errors of the oscilloscopes and DSA's and electrical signal travel time. These timing differences are resolved to within 0.3 ns of error. This along with the other category of uncontrollable independent error are listed below in Table A.1.

Table A.1 TIMING ERROR

1.	Synchronization	0.3 ns
2.	Oscilloscope (3% X 10ns) with 7B92A	0.3 ns
3.	Digitizing (.03%X 10 ns) signal analyzer	0.03 ns (1 ns res*)
4.	Digital interpretation by DCS	0.1 ns
5.	Digital Interpretation by DSA	0.01 ns
6.	Delay Generator	0.5 ns

*Though the accuracy is 0.03%, data points are only taken every nanosecond, so worst case error is actually 1 ns.

These timing errors are all independent so they can be added in quadrature. The resulting error is dependent upon which apparatuses are used in the measurement. The voltage - light onset time delays involve error sources 1 through 6 above thus resulting in an overall error of ±1.2 ns. Both the anode and cathode light signals are both measured on the same DSA, so comparison of their onset times thus involves only error sources 1, 3, 5, and 6. The resulting error then is ±1.15 ns rounded up to ±1.2 ns.

B. VOLTAGE MEASUREMENTS

Absolute signal strength was only important with the diode voltage signal because it was converted to actual diode voltage values using the method described in the experiment section of this paper. Since only relative signal strengths have any meaning for the light signals, no error analysis is necessary for the strength of the light signals. Sources of error for the diode voltage values determined in this experiment are shown in table A.2.

Table A.2 DIODE VOLTAGE ERROR

Oscilloscope vertical plug -in 7B92A	+/- 2%
Value of attenuation	+/- 5%
Digital interpretation by DCS w/ Zoom feature	+/- 1%

The diode voltage error sources listed in Table A.2 are independent so they can also be added in quadrature resulting in an overall diode voltage error of 5.47% rounded up to 6%. However, when attempting to determine the diode voltage at a certain instant in time, say at light onset, the timing error must be taken into account. This was accomplished by

estimating the slope of the voltage signal at the time of light onset, then estimating from this slope a voltage error based on the timing error involved. For the typical 55kV run the slope of the voltage signal was 0.05 V/ns with a ±1.2 ns timing error, this results in an oscilloscope voltage reading error of 0.06 V or with conversion to a diode voltage, we have a value of 19 kV. This must be added to a 6% error of the peak value of 1.83 V, (±0.11 V) oscilloscope error or a 35 kV diode voltage error. Summing the two we have a total error of ± 54 kV. The 75 kV shots have 3 V oscilloscope readings with slopes of about 0.2 V/ns. This results in a total error of 125 kV for the diode voltage at light onset. The 100 kV shots peak at 4 kV and have a slope of 0.4 V/ns, so the total diode voltage error is ±230 kV.

APPENDIX B: DATA

A. OPTICAL SETUP 1

Ten data runs and one dark or "Blackout" shot were taken for each charging voltage. The measured results of these shots are tabulated in tables B.1, B.2 and B.3.

Table B.1 55 KV MARX DATA (SETUP 1)

	Onsets(nanoseconds)			Time Differences		Oscope Voltage at
run	cathode	anode	volt	Cathode-Voltage	Cath-Anode	Light Onset
1	35	35	23	12	0	1.22
2	35	35	22.60	12.40	0	.93
3	41	40	30.30	10.70	-1	1.13
4	39	39	28.90	10.10	0	.80
5	45	45	35.50	9.50	0	1.22
6	50	50	38.60	11.40	0	1.38
7	52.50	52.50	43.30	9.20	0	1.51
8	53	53	43.10	9.90	0	1.58
9	52	52	42.70	9.30	0	1.39
10	53	53	44.20	8.80	0	1.40
11	Black out					
			Average	10.33	-.10	1.26
			STD DEV	1.25	.32	.27
			Avg diode voltage at light onset			401.76 kV
			Avg electric field at light onset			15.82 MV/m

Table B.2 75 KV MARX DATA (SETUP 1)

	Onsets(nanoseconds)			Time Differences		Oscope Voltage at	
run	cathode	anode	volt	Cathode-Voltage	Cath-Anode	Light Onset	
1	79	79	74.60	4.40	0	.90	
2	90.60	90.60	83.90	6.70	0	1.06	
3	81.80	81.80	77.20	4.60	0	.76	
4	85.60	85.60	78	7.60	0	1.29	
5	84	83	78.40	5.60	-1	.85	
6	81.40	81.40	75	6.40	0	.93	
7	84.40	84.40	78.40	6	0	1.10	
8	80.60	80.60	75.30	5.30	0	.61	
9	82	82	76.30	5.70	0	.82	
10	82.40	82.40	76.10	6.30	0	1.19	
11	Black out						
			Average	5.86	-.10	.95	
			STD DEV	.96	.32	67.73	kV
			Avg diode voltage at light onset			304.32	kV
			Avg electric field at light onset			11.98	MV/m

Table B.3 100 KV MARX DATA (SETUP 1)

	Onsets(nanoseconds)			Time Differences		Oscope Voltage at	
run	cathode	anode	volt	Cathode-Voltage	Cath-Anode	Light Onset	
1	39	39	33.90	5.10	0	1.07	
2	37	37	29.20	7.80	0	1.46	
3	38	38	32.90	5.10	0	1.12	
4	39	39	30.90	8.10	0	1.50	
5	38	38	31.10	6.90	0	1.48	
6	31	31	24.40	6.60	0	1.34	
7	38	38	31.50	6.50	0	1.43	
8	40	40	32.90	7.10	0	1.49	
9	39	39	32	7	0	1.50	
10	37	38	31.40	5.60	1	1.40	
11	Black out						
			Average	6.58	.10	1.38	
			STD DEV	1.04	.32	55.15	kV
			Avg diode voltage at light onset			441.28	kV
			Avg electric field at light onset			17.37	MV/m

B. OPTICAL SETUP 2

All data runs using optical setup 2 (with PVC disk) were accomplished on one day and in the following order 75 kV, 100kV, 55 kV and 85 kV. The raw data for these runs is listed in table B.4-B.6 below.

Table B.4 Data 85 kV setup 2

Cathode Onset (ns)	Anode Onset (ns)	Peaks (mV) Cathode	Anode
21	22	7	7
----------switched detectors---------			
21	23	3	7
AVG Time diff.		**AVG Peaks** 5	7
Cath VS Anode:	1.5 ns		

Table B.5 Data 100 kV Setup 2

Cathode Onset (ns)	Cathode Ramp (ns)	Anode onset (ns)	Peaks (mV) Cathode	Anode
25	28	28	16	24
----------	switched detectors	----------		
61	--	63	7	21

AVG Time Differences
Cath VS Anode: 2.5 ns

AVG Peaks **12** **23**

Table B.6 Data 75 kV Setup 2

Cathode onset (ns)	Anode ramp (ns)	Peaks (mV) onset (ns)	Cath.	Anode
60	61	62	386	27
40	42	42	362	18
29	30	30	218	13
28	30	31	229	11
51	52	52	362	15
----------	switched detectors	----------		
50	51	51	358	14
51	52	53	374	13
52	53	53	331	12
49	50	49	374	12
51	52	51	373	11
AVG Time Differences		**AVG peak**	**321**	**15**
Cath VS Anode: 1.25 ns				
C.Ramp VS Anode: .083 ns				

Table B.7 Data 55 kV setup 2

Cathode Onset (ns)	Cathode Ramp (ns)	Anode Onset (ns)	Peaks (mV) Cath.	Anode
12	13	14	171	1.2
39	40	41	171	1.7
38	39	39	72	2.4
----------	switched detectors		----------	
39	--	40	50	1.2
38	40	39	50	3.2

AVG Time Differences **AVG Peaks** 63 2
Anode VS Cathode: 1.4 ns
Anode VS C. Ramp: .2 ns

LIST OF REFERENCES

1. Parker, R., *Explosive Electron Emission and the Characteristics of High Current Flow*, Air force Weapons Laboratory, Kirtland Air Force Base, N.M., 1974.

2. Schwirzke, F. "Formation of Cathode Spots by Unipolar Arcing " in *Gaseous Dielectrics VI*, Ed. L.G. Christophorou and I. Sauers, Plenum Press, New York, 1991.

3. Hallal, M. P. Jr., *The onset of Breakdown in a Fast Pulsed Vacuum Diode*, Master's Thesis, Naval Postgraduate School, Monterey, California, June 1992.

4. Willis, G., *Investigation of Onset of Plasma Formation at Anode of Fast Pulsed High Voltage Vacuum Diode*, Master's Thesis, Naval Postgraduate School, March 1993.

5. Mesyats, G. A., and Proskurovsky, D.I., *Pulsed Electrical Discharge in Vacuum*, Springer-Verlag, 1989.

6. Kittel, C. and Kroemer H., *Thermal Physics* 2nd ed. W.H. Freeman and Company, New York, 1980.

7. Barnett, C., Ray, J., and Thompson, J., *Atomic and Molecular Collision Cross Sections of Interest in Controlled Thermonuclear Research*, pp.138-141, Oak Ridge National Laboratory, August 1964.

8. Glarawicz, D., *Instrumentation Requirements for Tree Effects Data Collection at the Naval Postgraduate School Flash X-ray Facility*, Master's Thesis, Naval Postgraduate School, Monterey, California, June 1990.

9. Physics International Company, *Model 112A Pulserad Pulsed X-ray Generator Operations and Maintenance Mantel, January, 1986.*

10. New Focus Inc., *User's Mantel, Model 1601 Low Noise Photoreceiver*, 1992.

11. Fast Pulse Lasermetrics Inc., *Operator's Manuel Series 3117, TYPE I*, 1984.

12. Tektronix Inc., *User's Manual 7104 Oscilloscope*, 1986.

13. Tektronix Inc., *DCS01 Digitizing Camera System Software*, 1988.

14. Tektronix Inc., *User's Manuel DSA 602A*, 1992.

15. Pietruszka, R.B, *Operation and Characteristics of the Flash X-ray Generator at Naval Postgraduate School*, Master's Thesis, Naval Postgraduate School, Monterey, California, June 1991.

16. Callahan, M., *X-ray Pulse Considerations and Electron Flow in High Voltage Diodes*, Master's Thesis, Naval Postgraduate School, Monterey, California, December 1993.

INITIAL DISTRIBUTION LIST

		No. Copies
1.	Defense Technical Information Center Cameron Station Alexandria VA 22304-6145	2
2.	Library, Code 052 Naval Postgraduate School Monterey CA 93943-5002	2
3.	Professor Fred Schwirzke, Code PH/Sw Department of Physics Naval Postgraduate School Monterey CA 93943-5000	2
4.	Professor Xavier K. Maruyama, Code PH/Mx Department of Physics Naval Postgraduate School Monterey CA 93943-5000	2
5.	Professor William B. Colson, Code PH/Cw Chairman, Department of Physics Naval Postgraduate School Monterey CA 93943-5000	1
6.	Physics Library, Code PH Department of Physics Naval Postgraduate School Monterey CA 93943-5000	1
7.	CPT Charles M. Wright 19330 Whispering Pines Rd. Miami, FL 33157	2